

## NASA's *Pandora SmallSat Mission*: Simulated Modeling and Retrieval of Near-Infrared Exoplanet Transmission Spectra

YOAV ROTMAN <sup>1,2</sup> PETER MCGILL <sup>1</sup> LUIS WELBANKS <sup>2</sup> BENJAMIN V. RACKHAM <sup>3,4</sup> AISHWARYA IYER <sup>5,\*</sup>  
DÁNIEL APAI <sup>6,7</sup> MICHAEL R. LINE <sup>2</sup> ELISA V. QUINTANA <sup>5</sup> JESSIE L. DOTSON <sup>8</sup> KNICOLE D. COLÓN <sup>5</sup>  
THOMAS BARCLAY <sup>5</sup> CHRISTINA HEDGES <sup>5,9</sup> JASON F. ROWE <sup>10</sup> EMILY A. GILBERT <sup>11</sup> BRETT M. MORRIS <sup>12</sup>  
JESSIE L. CHRISTIANSEN <sup>13</sup> TREVOR O. FOOTE <sup>5,\*</sup> AYLIN GARCÍA SOTO <sup>14</sup> THOMAS P. GREENE <sup>13</sup>  
KELSEY HOFFMAN <sup>10</sup> BENJAMIN J. HORD <sup>5,\*</sup> AURORA Y. KESSELI <sup>13</sup> VESELIN B. KOSTOV <sup>5,15</sup>  
MEGAN WEINER MANSFIELD <sup>16</sup> AND LINDSEY S. WISER <sup>17</sup>

<sup>1</sup>*Space Science Institute, Lawrence Livermore National Laboratory, 7000 East Ave., Livermore, CA 94550, USA*

<sup>2</sup>*School of Earth and Space Exploration, Arizona State University, Tempe, AZ, USA*

<sup>3</sup>*Department of Earth, Atmospheric and Planetary Sciences, Massachusetts Institute of Technology, Cambridge, MA 02139, USA*

<sup>4</sup>*Kavli Institute for Astrophysics and Space Research, Massachusetts Institute of Technology, Cambridge, MA 02139, USA*

<sup>5</sup>*NASA Goddard Space Flight Center, 8800 Greenbelt Road, Greenbelt, MD 20771, USA*

<sup>6</sup>*Steward Observatory, The University of Arizona, Tucson, AZ 85721, USA*

<sup>7</sup>*Lunar and Planetary Laboratory, The University of Arizona, Tucson, AZ 85721, USA*

<sup>8</sup>*NASA Ames Research Center, MS 245-6, Moffett Field, CA 94035, USA*

<sup>9</sup>*University of Maryland, Baltimore County, 1000 Hilltop Circle, Baltimore, Maryland, United States*

<sup>10</sup>*Department of Physics and Astronomy, Bishops University, 2600 Rue College, Sherbrooke, QC J1M 1Z7, Canada*

<sup>11</sup>*Jet Propulsion Laboratory, California Institute of Technology, 4800 Oak Grove Drive, Pasadena, CA 91109, USA*

<sup>12</sup>*Space Telescope Science Institute, 3700 San Martin Drive, Baltimore, MD 21218, USA*

<sup>13</sup>*California Institute of Technology/IPAC, 1200 California Blvd, MC 100-22, Pasadena, CA 91125, USA*

<sup>14</sup>*Department of Physics and Astronomy, Dartmouth College, Hanover NH 03755, USA*

<sup>15</sup>*SETI Institute, 189 Bernardo Ave, Suite 200, Mountain View, CA 94043, USA*

<sup>16</sup>*Department of Astronomy, University of Maryland, 4296 Stadium Drive, College Park, MD 20742, USA*

<sup>17</sup>*Johns Hopkins University Applied Physics Laboratory, 11100 Johns Hopkins Rd, Laurel, MD 20723, USA*

### ABSTRACT

Pandora is a SmallSat mission dedicated to understanding exoplanets and their host stars by disentangling the impact of stellar heterogeneity on exoplanet transmission spectra. Selected as a NASA Astrophysics Pioneers mission in 2021, Pandora will provide simultaneous long-term visible photometric monitoring (0.4–0.7  $\mu\text{m}$ ) and low-resolution near-infrared (NIR) spectroscopy (0.9–1.6  $\mu\text{m}$ ) of transiting systems for the purposes of monitoring host star variability and characterizing exoplanetary atmospheres. Pandora's year-long prime mission from 2026 to 2027 coincides with the middle of a decade defined by targeted efforts for atmospheric characterization of exoplanets, offering a key opportunity to leverage this new resource to maximize science with JWST and other observatories. Here we investigate Pandora's anticipated performance for the general exoplanet population accessible to transit spectroscopy, from hot Jupiters to temperate sub-Neptunes. By modeling the atmospheres of five test cases broadly consistent with the bulk properties of HD 209458 b, HD 189733 b, WASP-80 b, HAT-P-18 b, and K2-18 b, we find that Pandora may provide abundance constraints as precise as  $\sim 1.0$  dex for main atmospheric absorbers such as H<sub>2</sub>O and CH<sub>4</sub>. Then, we explore the synergies between Pandora and JWST. Our results suggest that targets with JWST data in the near-infrared can benefit from the addition of Pandora observations and result in more reliable abundance estimates than with JWST data alone. Moreover, Pandora can serve the community by providing precursory observations of targets of interest for JWST atmospheric characterization. We conclude by outlining strategies for the use of Pandora as a standalone observatory and in synergy with JWST.

\* NASA Postdoctoral Fellow

## 1. INTRODUCTION

The compositions of exoplanets offer unique insights into their formation and evolution, making compositional inferences a key scientific goal over the last two decades. These constraints typically come from transmission spectroscopy: as a planet transits its host star, the absorption spectrum of its atmosphere is imprinted into the observed stellar spectrum (S. Seager & D. D. Sasselov 2000). Extracting the atmospheric spectrum then allows us to make quantitative inferences about its temperature structure, chemical inventory, and aerosols. These inferences, in turn, inform us about the planet’s formation and evolutionary history (e.g., K. I. Öberg et al. 2011; N. Madhusudhan 2012; C. Mordasini et al. 2016).

The *James Webb Space Telescope* (JWST; J. P. Gardner et al. 2006) has revolutionized the field of transmission spectroscopy, providing spectra of exoplanet atmospheres with wider wavelength coverage ( $\sim 0.6\text{--}12.5\ \mu\text{m}$ ) and a higher resolution than any previous space-based observatory. JWST observations have enabled new insights into exoplanet atmospheres (see, e.g., N. Espinoza & M. D. Perrin 2025), including the first detections of carbon-bearing species (e.g., JWST Transiting Exoplanet Community Early Release Science Team et al. 2022; T. J. Bell et al. 2023) and photochemical processes (e.g., S.-M. Tsai et al. 2023). JWST spectra have also ushered in higher-precision constraints on the atmospheric chemical inventory (e.g., L. Welbanks et al. 2024; T. G. Beatty et al. 2024) as well as clouds and hazes (e.g., A. Dyrek et al. 2024; J. Inglis et al. 2024).

JWST’s increased precision, however, has also highlighted the effects of stellar contamination on the planetary spectrum (e.g., G. Fu et al. 2022; S. E. Moran et al. 2023; M. Fournier-Tondreau et al. 2024a,b; C. I. Cañas et al. 2025), where heterogeneity in the stellar surface imprints stellar spectral features into the observed transmission spectrum through the transit light source (TLS) effect (B. V. Rackham et al. 2018, 2019). While occulted starspots can be identified and corrected in the transit light curve (e.g., F. Pont et al. 2013), unocculted spot modulation is often harder to definitively identify in the host star. If uncorrected, this effect can cause significant biases in analyses of transmission spectra (A. Pinhas et al. 2018; A. R. Iyer & M. R. Line 2020; B. V. Rackham et al. 2023; B. V. Rackham & J. de Wit 2024). This issue is particularly pronounced for observations of small, rocky planets around K and M dwarfs. While these low-mass host stars are the most accessible to transit spectroscopy of small planets (O. Lim et al. 2023; M. Radica et al. 2025), they are known to have higher levels of magnetic activity (e.g., P. S. Muirhead et al. 2018),

leading to more heterogeneities on the stellar surface. Although stellar contamination of transmission spectra is not unique to JWST observations (e.g., F. Pont et al. 2008, 2013; P. R. McCullough et al. 2014; B. Rackham et al. 2017; Z. Zhang et al. 2018), it has become the major limitation for interpreting JWST transmission spectra, and often prevents confident identification of exoplanetary atmospheres (e.g., S. E. Moran et al. 2023).

Pandora is a SmallSat Mission selected by NASA in 2021 as part of the Astrophysics Pioneers Program (E. V. Quintana et al. 2021, 2024; T. Barclay et al. 2025), and launched in January 2026. It is designed to address the challenge of the stellar contamination by combining near-IR spectroscopy ( $\sim 0.9\text{--}1.6\ \mu\text{m}$ ;  $R \gtrsim 30$ ) with simultaneous visible-light photometry ( $\sim 0.4\text{--}0.7\ \mu\text{m}$ ) for twenty transiting exoplanet systems (T. O. Foote et al. 2022). Pandora has a 0.45 meter diameter primary mirror, and allows both wavelength channels to operate simultaneously. The bandpass of Pandora’s Near-Infrared Detector Assembly (NIRDA) instrument covers multiple absorption bands of  $\text{H}_2\text{O}$ , which is ubiquitous in exoplanet atmospheres, but can also trace star spots (B. V. Rackham et al. 2018, 2019). By combining time-resolved, long-baseline optical photometry and NIR spectroscopy, Pandora will enable the disentanglement of stellar variability from planetary spectra, allowing for accurate inferences from both the planets and their host stars (K. Hoffman et al. 2022). Pandora is expected to observe  $\sim 20$  primary mission targets, and capture a baseline of at least ten transits for each target, throughout its mission lifetime.

In this work, we assess Pandora’s capabilities for atmospheric characterization and examine how observations from Pandora and JWST combined can improve the accuracy and precision of atmospheric inferences. We simulate synthetic spectra of five benchmark exoplanets and perform atmospheric retrievals using both observatories to analyze the expected accuracy and precision for each target and instrument combination. In Section 2, we describe our target selection, synthetic data simulation, and retrieval methodology. In Section 3, we describe the observational capabilities of Pandora. In Section 4, we analyze possible uses for joint observations between JWST and Pandora, and which instruments and targets benefit most from synergistic observations. Finally, in Section 5, we summarize our findings and recommend future considerations when observing exoplanets with both observatories.

Planet	$R_p$ [ $R_J$ ]	$M_p$ [ $M_J$ ]	$T_{\text{eq}}$ [K]	$R_*$ [ $R_\odot$ ]	$M_*$ [ $M_\odot$ ]	$T_{\text{eff}}$ [K]
HD 209458 b <sup>a</sup>	$1.380 \pm 0.015$	$0.714 \pm 0.014$	$1459 \pm 12$	$1.162 \pm 0.012$	$1.148 \pm 0.040$	$6117 \pm 50$
HD 189733 b <sup>b</sup>	$1.142^{+0.036}_{-0.034}$	$1.130^{+0.047}_{-0.045}$	$1220 \pm 13$	$0.777 \pm 0.001$	$0.840^{+0.099}_{-0.112}$	$5053^{+46}_{-45}$
WASP-80 b <sup>c</sup>	$0.999^{+0.030}_{-0.031}$	$0.538^{+0.035}_{-0.036}$	$825 \pm 19$	$0.586^{+0.017}_{-0.018}$	$0.577^{+0.051}_{-0.054}$	$4143^{+92}_{-94}$
HAT-P-18 b <sup>d</sup>	$0.995 \pm 0.052$	$0.197 \pm 0.013$	$852 \pm 28$	$0.749 \pm 0.037$	$0.770 \pm 0.031$	$4803 \pm 80$
K2-18 b <sup>e,f</sup>	$0.232 \pm 0.008$	$0.027 \pm 0.004$	$255 \pm 4$	$0.445 \pm 0.015$	$0.495 \pm 0.004$	$3457 \pm 39$

**Table 1.** System parameters for our five selected targets. We adopt the median of the reported system parameters for our models. **References:** a) J. Southworth (2010); b) B. Addison et al. (2019); c) A. H. M. J. Triaud et al. (2015); d) J. D. Hartman et al. (2010); e) B. Benneke et al. (2019); f) R. Cloutier et al. (2019).

## 2. SIMULATING AND RETRIEVING TRANSMISSION SPECTRA

We simulate synthetic transmission spectra for five exoplanet targets with the Aurora framework (L. Welbanks & N. Madhusudhan 2021), modeling observations for the Pandora NIR detector and the Near-Infrared Camera (NIRCam) instrument on JWST. We select NIRCam due to its complimentary wavelength range; while Pandora covers the 0.9–1.6  $\mu\text{m}$  band, NIRCam’s long-wavelength channel covers 2.4–5.1  $\mu\text{m}$ , allowing for a wider wavelength coverage encompassing more absorption features. We then use the Bayesian inference methodology known as “atmospheric retrieval” (e.g., N. Madhusudhan & S. Seager 2009) to assess inferences from Pandora alone and in combination with JWST. Throughout this work, we assume that the observed spectra have already been corrected for stellar contamination, so that the data represents a planetary spectrum in the case of an ideal star. Companion studies will examine Pandora’s ability to constrain stellar photospheric heterogeneity and mitigate the TLS effect (B. V. Rackham et al. 2026). Here, we describe our target selection, forward models, and retrieval methodologies.

### 2.1. Targets

Our study aims to explore Pandora’s performance for the general exoplanet population currently accessible for atmospheric characterization with transit spectroscopy. We broadly model this population by simulating the atmospheres of five targets spanning the hot Jupiter to temperate sub-Neptune regime. The cases selected broadly follow the bulk properties of HD 209458 b, HD 189733 b, WASP-80 b, HAT-P-18 b, and K2-18 b (i.e., mass, radius, equilibrium temperature, and host star, see Table 1)<sup>1</sup>. The atmospheric compositions

adopted in Section 3 generally follow existing constraints from the literature as described below, whereas those in Section 4 are motivated by chemical equilibrium expectations for an enhanced metallicity atmosphere. Below we describe the context of each planet archetype adopted in our study.

#### 2.1.1. HD 209458 b

HD 209458 b is a hot Jupiter orbiting a G0V star. It holds a unique spot as the first discovered transiting exoplanet and the first to have its atmosphere characterized (D. Charbonneau et al. 2000, 2002; A. Vidal-Madjar et al. 2003, 2004). It is a uniquely well-suited target for transmission spectroscopy studies, with HST (e.g., D. Deming et al. 2013; D. K. Sing et al. 2016), *Spitzer* (e.g., T. M. Evans et al. 2015), JWST (e.g., Q. Xue et al. 2024), and ground-based observations (e.g., P. Giacobbe et al. 2021). The atmosphere of HD 209458 b shows signs of water (D. Deming et al. 2013), clouds and hazes (D. K. Sing et al. 2016), and more recently, evidence of carbon and sulfur bearing molecules (P. Giacobbe et al. 2021; Q. Xue et al. 2024).

#### 2.1.2. HD 189733 b

HD 189733 b is a hot Jupiter orbiting a K2 dwarf (F. Bouchy et al. 2005). Like HD 209458 b, it has been extensively studied, with observations from both ground- (e.g., S. Redfield et al. 2008; M. Brogi & M. R. Line 2019) and space-based observatories (e.g., D. Charbonneau et al. 2008; E. Agol et al. 2010). Recent JWST observations of the transmission spectrum have identified H<sub>2</sub>O, CO, CO<sub>2</sub>, H<sub>2</sub>S, and SiO<sub>2</sub> (G. Fu et al. 2024; J. Inglis et al. 2024), while previous HST observations showed signs of H<sub>2</sub>O, haze-induced scattering, and unocculted starspots (e.g., F. Pont et al. 2008, 2013; A. Lecavelier des Etangs et al. 2008; D. K. Sing et al. 2009). Moreover, previous studies have suggested strong stellar activity from HD 189733 (e.g., E. Miller-Ricci et al. 2008; F. Pont et al. 2008, 2013; P. R. McCullough et al.

<sup>1</sup> We note that both WASP-80 b and HAT-P-18 b are among the Pandora primary mission targets, see <https://pandorasat.com/targets/>

2014; I. S. Narrett et al. 2024), making it a strong candidate for Pandora observations.

### 2.1.3. WASP-80 b

WASP-80 b is a warm Jupiter orbiting a low-mass late K dwarf (A. H. M. J. Triaud et al. 2013). It straddles the lower edge of the warm Jupiter temperature range ( $T_{\text{eq}} = 825$  K), making it a unique testbed for atmospheric chemistry in cooler Jovians. WASP-80 b has been observed with HST (e.g., I. Wong et al. 2022; B. Jacobs et al. 2023) and JWST (e.g., T. J. Bell et al. 2023; L. S. Wisner et al. 2025), as well as various ground-based observations (e.g., A. Fukui et al. 2014; L. Mancini et al. 2014; I. Carleo et al. 2022), leading to detections of  $\text{H}_2\text{O}$  and carbon-bearing species, alongside possible aerosol contributions from clouds.

### 2.1.4. HAT-P-18 b

HAT-P-18 b is a low-density warm Saturn orbiting a K2 dwarf. Like WASP-80 b, the low temperature of HAT-P-18 b ( $T_{\text{eq}} = 852$  K) makes it an enticing target for understanding giant planet chemistry. Since its original discovery (J. D. Hartman et al. 2010), HAT-P-18 b has been observed by both ground-based (e.g., J. Kirk et al. 2017) and space-based observatories (e.g., A. Tsiaras et al. 2018), leading to the detection of a Rayleigh scattering slope, water absorption, and possible cloud and haze contributions to the transmission spectrum. More recently, HAT-P-18 b was an Early Release Observation (ERO) target for JWST, with NIRISS observations leading to detections of  $\text{H}_2\text{O}$ ,  $\text{CO}_2$ , He, and a high-altitude cloud deck, with signatures of Na (G. Fu et al. 2022; M. Fournier-Tondreau et al. 2024a).

### 2.1.5. K2-18 b

K2-18 b is a temperate sub-Neptune orbiting a K2 dwarf (B. T. Montet et al. 2015). K2-18 b has been observed with JWST across the near- to mid-IR, with NIRSpec, NIRISS, and MIRI observations. HST/WFC3 observations yielded an  $\text{H}_2\text{O}$  detection with negligible  $\text{CH}_4$  (B. Benneke et al. 2019; A. Tsiaras et al. 2019; L. Welbanks et al. 2019; N. Madhusudhan et al. 2020), though follow-up observations with JWST detected  $\text{CH}_4$  and  $\text{CO}_2$ , with only upper limit constraints on  $\text{H}_2\text{O}$ , and a strong super-Rayleigh slope (N. Madhusudhan et al. 2023; R. Hu et al. 2025).

## 2.2. Atmospheric Model

We use Aurora (L. Welbanks & N. Madhusudhan 2021), an exoplanet atmospheric spectra forward modeling and retrieval framework, to simulate the atmospheres of each target. Aurora solves radiative transfer

assuming hydrostatic equilibrium and a plane-parallel one-dimensional atmosphere to produce the transmission spectrum of the planet. We assume an isothermal atmosphere at the equilibrium temperature of each planet in our models. The synthetic observations are the result of a planetary atmospheric model only; i.e., there is no spectroscopic contribution due to a heterogeneous stellar photosphere and the TLS effect.

In Section 3, we present an investigation into the constraining power of Pandora’s NIRDA detector. We build each planetary model based broadly on inferences from previous JWST observations and expectations from chemical equilibrium, including absorption contributions from  $\text{H}_2\text{O}$ ,  $\text{CH}_4$ ,  $\text{CO}$ ,  $\text{CO}_2$ ,  $\text{H}_2\text{S}$ ,  $\text{NH}_3$ , Na, and K. Additionally, we account for inhomogeneous cloud coverage along the terminator using a linear model combination of cloudy and cloud-free models (M. R. Line & V. Parmentier 2016). We treat cloud coverage as an opaque gray slab at pressure  $P_{\text{cloud}}$  (e.g., A. Pinhas et al. 2018), and treat any haze scattering slope as an enhancement to  $\text{H}_2$  Rayleigh scattering (e.g., A. Lecavelier des Etangs et al. 2008); this includes two parameters representing the scattering slope  $\gamma$  (where  $\gamma = -4$  for pure Rayleigh scattering) and a multiplicative enhancement term,  $a$ .

In Section 4, we compare observations with Pandora to those done in tandem with JWST/NIRCam. We model our selected planets, adopting the bulk parameters in Table 1 and assume an atmosphere with  $\text{H}_2\text{O}$ ,  $\text{CH}_4$ ,  $\text{CO}$ , and  $\text{CO}_2$ ; we select abundances consistent with a solar C/O ratio and  $10\times$  solar metallicity at the equilibrium temperature of each of our targets (J. I. Moses et al. 2013), and limit our absorbers to carbon- and oxygen-bearing species. Though these abundances may differ from the literature values, we choose these to homogenize our sample. This allows for considerations of future target selection and refinement, particularly for targets without current JWST observations. Additionally, we assume a cloud-free atmosphere with Rayleigh scattering for each target, as we are interested in the combined ability of Pandora and JWST to provide more accurate constraints on the atmospheric C and O abundances.

We adopt line-lists for  $\text{H}_2\text{O}$ ,  $\text{CO}$ ,  $\text{CO}_2$  (L. S. Rothman et al. 2010),  $\text{CH}_4$  (S. N. Yurchenko & J. Tennyson 2014),  $\text{NH}_3$  (S. N. Yurchenko et al. 2011),  $\text{H}_2\text{S}$ ,  $\text{SO}_2$  (D. S. Underwood et al. 2016), Na (N. F. Allard et al. 2019), and K (N. F. Allard et al. 2016), as well as collision-induced absorption from  $\text{H}_2$ - $\text{H}_2$  and  $\text{H}_2$ -He scattering (C. Richard et al. 2012). The absorption cross sections, as well as the bandpasses of Pan-

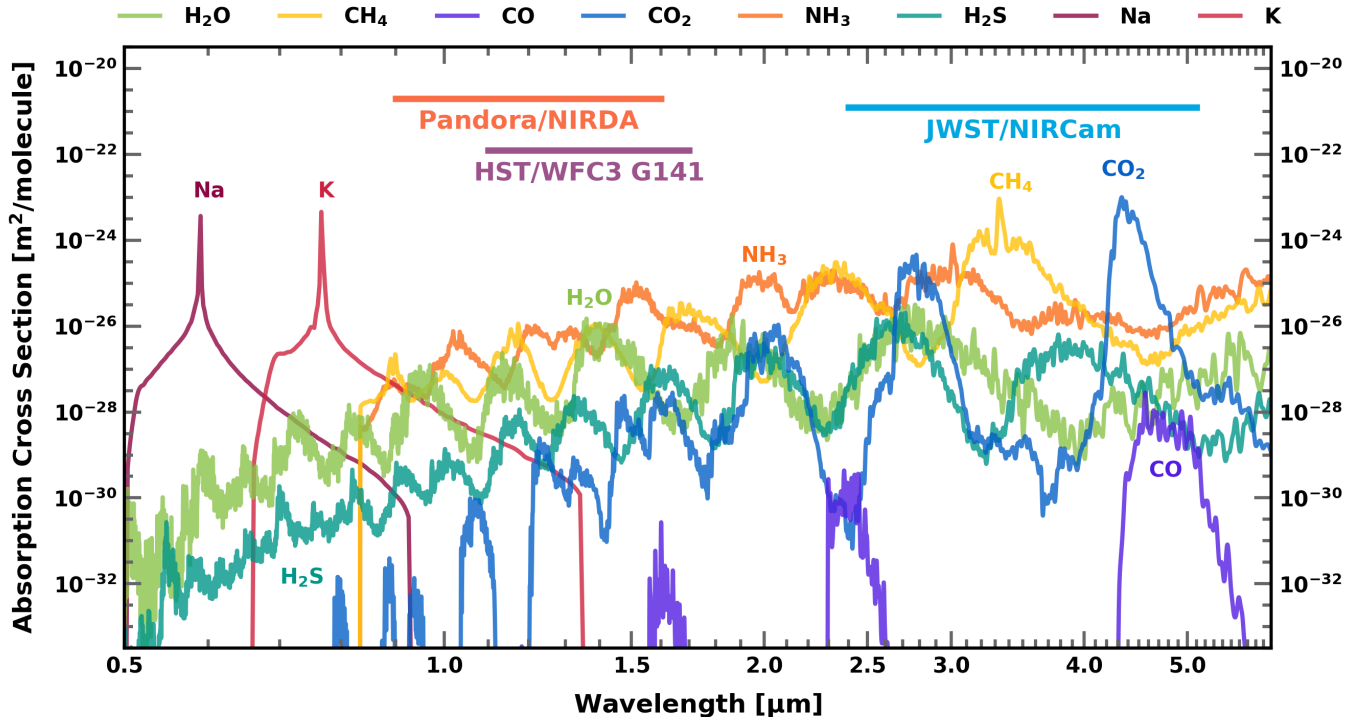


**Figure 1.** The absorption cross sections of common absorbers in exoplanet atmospheres considered in this work, shown at a pressure and temperature of 0.1 mbar and 1000 K. The wavelength coverage of Pandora’s NIR detector (NIRDA), JWST’s NIRCcam F322W2 and F444W filters, and HST’s WFC3 instrument (for the G141 grism) are shown. Pandora/NIRDA covers absorption bands of H<sub>2</sub>O, CH<sub>4</sub>, NH<sub>3</sub> and the wing of the K doublet, making it most sensitive to these absorbers.

dora, HST/WFC3/G141, and the JWST/NIRCcam long-wavelength filters are shown in Figure 1.

We use Aurora to perform our atmospheric retrievals on the data. Retrievals combine Bayesian inference sampling (via MultiNest; F. Feroz et al. 2009; J. Buchner et al. 2014) and forward models to quantitatively place constraints on atmospheric parameters from exoplanetary spectra. By identifying the region of parameter space that maximizes the Bayesian likelihood, retrievals provide posterior probability distributions for the model parameters that govern the transmission spectrum, giving insight into the thermochemical state of the atmosphere. For a review of atmospheric retrieval techniques and models, see, e.g., N. Madhusudhan (2018). Here, we use 500 live points for our sampling, with a 100-layer atmospheric pressure grid and a spectral resolution of 10,000. A full table of the assumed absorbers, atmospheric temperatures, and cloud and haze profiles, as well as the Bayesian priors used throughout this work, are given in Tables 2 (for Section 3) and 3 (for Section 4) in Appendix A.

### 2.3. Synthetic Pandora and JWST Observations

For each target, we simulate observations of the transmission spectrum with Pandora’s NIR detector and

JWST/NIRCcam (for both the F322W2 and F444W filters). For planets with published JWST NIRCcam observations (HD 209458 b, HD 189733 b, and WASP-80 b), we adopt the published bins, bin widths, and uncertainties of the JWST data. For those without existing observations (HAT-P-18 b, K2-18 b, and F444W observations of WASP-80 b), we use the PandExo precision calculator (N. E. Batalha et al. 2017), and bin the observations to  $R = 200$ . We simulate astrophysical and instrument noise in each observation by normally scattering each synthetic data point.

We simulate the estimated uncertainty for Pandora’s NIR observations following T. P. Greene et al. (2016). To calculate the signal-to-noise ratio (SNR) in each spectral bin, we use the `pandora-sat`<sup>2</sup> Python package, developed by the Pandora team to simulate Pandora’s performance (C. Hedges et al. 2024). We first calculate the observed SED of a given host star, modeled using an interpolated PHOENIX (T. O. Husser et al. 2013) model and the NIRDA instrument sensitivity and resolution (average  $R \approx 110$ ). We then integrate the product of the stellar SED and the instrument sensitivity along each

<sup>2</sup> Package publicly available at <https://github.com/PandoraMission/pandora-sat/>

wavelength bin to calculate the observed flux per bin. From this, we calculate the photon shot noise of the observation, as well as the detector read and dark noise (from *pandora-sat*), to estimate the SNR of each spectral bin, which we convert to an associated uncertainty.

For each target, we model a total observation time of twice the ingress to egress time ( $T_{14}$ ) of the planet. This corresponds to a full transit observation and an equal out-of-transit baseline observation of the star. Given Pandora’s low Earth orbit, it will be difficult to obtain uninterrupted observations of the entire transit (similar to observations with HST). We therefore assume a 50% duty cycle, approximating that an average target will be inaccessible for roughly half of the observation time. We note that Pandora will observe each primary mission target for a 24 hour visit, which will provide a longer out-of-transit baseline and likely lead to better SNR. We assume a wavelength-independent 5-pixel width for the PSF and do not consider possible effects from spacecraft jitter or noise from signals of nearby background stars, which can increase the uncertainty and introduce correlated noise (e.g., D. K. Sing et al. 2011).

We bin our synthetic Pandora observations to  $R \approx 30$  (following K. Hoffman et al. 2022). For multiple observations, we assume that the uncertainties can be defined as decreasing by a factor of  $\sqrt{N_{\text{trans}}}$ , representing the increase in SNR with multiple observations. This represents the optimistic scenario, in which our uncertainties are dominated by photon noise. In Figure 2, we show the estimated range of uncertainties for one, five, ten, and twenty stacked Pandora observations, each with a five hour total integration time, for a warm Jupiter-like system with varying J band stellar magnitude.

### 3. PANDORA’S OBSERVATIONAL CAPABILITIES

Pandora’s NIRDA instrument covers a similar wavelength range ( $\sim 0.9\text{--}1.6\ \mu\text{m}$ ) to the G141 grism of HST/WFC3 ( $\sim 1.1\text{--}1.7\ \mu\text{m}$ ); the latter has detected  $\text{H}_2\text{O}$  absorption in exoplanet atmospheres (e.g., D. Deming et al. 2013; H. R. Wakeford et al. 2017, 2018), alongside terminator clouds and hazes (e.g., F. Pont et al. 2013; D. K. Sing et al. 2016). With multiple dedicated observations per target, Pandora is expected to provide constraints similar to those of HST. Here we explore Pandora’s observational capabilities with NIRDA, in order to identify the expected scientific output and the number of observations needed for atmospheric characterization.

#### 3.1. Constraining Atmospheric Composition of Primary Mission Targets

Pandora is expected to observe ten transits as a preliminary baseline for each of its primary mission targets

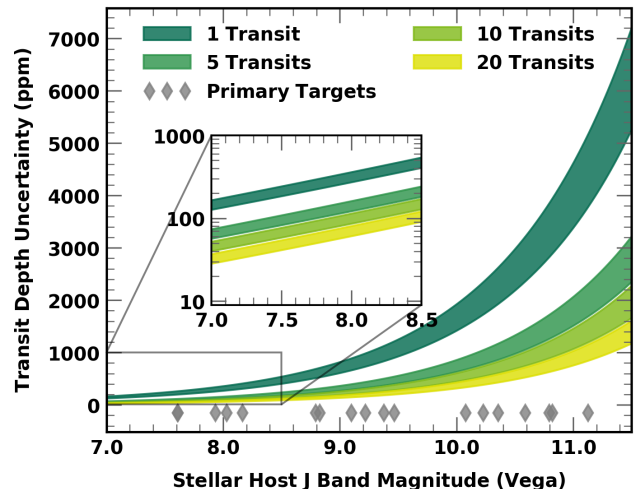


**Figure 2.** The range of uncertainties predicted by our calculations for Pandora observations of a warm Jupiter-like system (here, WASP-80 b) with varying stellar magnitude, after binning to  $R \simeq 30$ . Different stellar fluxes and detector properties at different wavelengths will lead to different uncertainties throughout the bandpass; the bands here represent the range between the lowest and highest uncertainties. Stacking multiple observations will provide lower uncertainties, particularly for fainter targets. The inset shows the uncertainties for brighter stars, for which Pandora can achieve precisions as low as  $\sim 30$  ppm when multiple transits are observed. The magnitudes of stars included in the Pandora primary target list are shown as diamonds.

(K. Hoffman et al. 2022). We generate synthetic Pandora observations with uncertainties reflecting the expected precision from ten transit observations following the description in Section 2.2. As our targets represent the region of planetary parameter space probed by Pandora’s primary mission targets, we aim to identify which absorbers and atmospheric properties will be best constrained by Pandora observations, and whether ten transits will be sufficient for primary mission targets.

For each target in Section 2.1, we generate a model of the atmospheric spectrum based on previous observations and Pandora’s instrumental properties. The full list of parameters used in generating the forward models is given in Table 2 in Appendix A. The forward models and synthetic data for ten transit observations with Pandora are shown in Figure 3.

We analyze two forms of each forward model; a “simple” cloud- and haze-free model comprised of absorbers in the Pandora bandpass ( $\text{H}_2\text{O}$ ,  $\text{CH}_4$ , and  $\text{NH}_3$ ) and a “comprehensive” model that includes partial clouds, hazes, and species that do not have strong absorption lines in the Pandora bandpass (e.g.,  $\text{CO}$  and  $\text{CO}_2$ ). A full list of absorbers in the comprehensive model is provided in Table 2 in Appendix A.

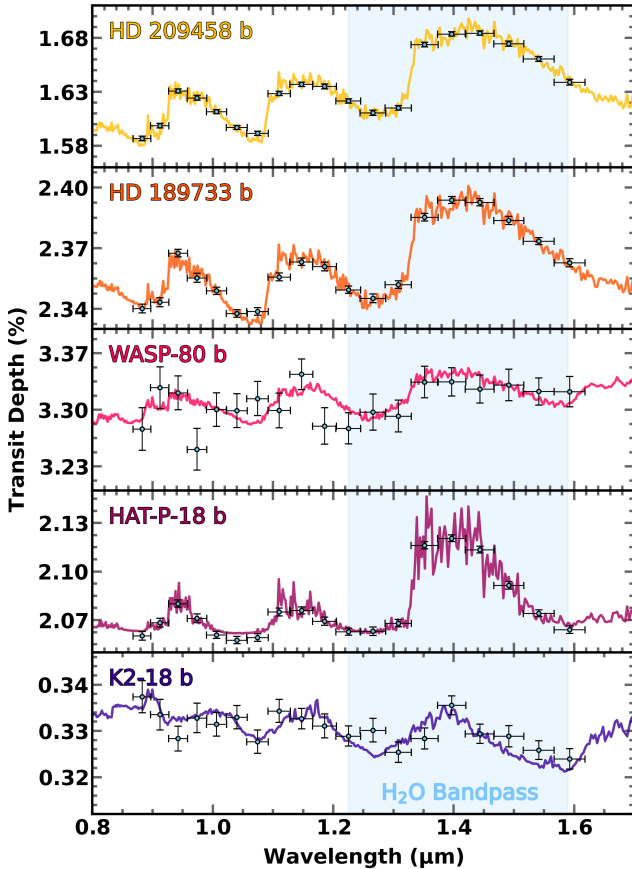


**Figure 3.** Synthetic forward models and observations with Pandora’s NIRDA instrument of the five targets. The data is binned to a resolution of  $R \simeq 30$ , and error bars are simulated for ten transit observations. The  $1.4 \mu\text{m}$  water absorption band is highlighted for reference, though K2-18 b shows a similar feature from  $\text{CH}_4$  absorption.

### 3.1.1. Molecular Abundances

We find that, for most of our targets, Pandora is able to provide constraints on  $\text{H}_2\text{O}$  abundance of  $\lesssim 1$  dex, comparable to HST constraints (e.g., A. Tsiaras et al. 2018). For K2-18 b, the water is unconstrained with only an upper limit, consistent with inferences from JWST, which found a  $\text{CH}_4$ -dominated atmosphere (e.g., N. Madhusudhan et al. 2023; R. Hu et al. 2025); additionally, WASP-80 b is the faintest target considered in this work and has a high altitude obscuring cloud deck (T. J. Bell et al. 2023), leading to a wider and less informative  $\text{H}_2\text{O}$  posterior distribution. For particularly cloudy planets like HAT-P-18 b and WASP-80 b, we find inferences broadly consistent with the true  $\text{H}_2\text{O}$  abundance with precisions of  $\sim 2$  dex. The posterior probability distributions of  $\text{H}_2\text{O}$  abundance in both the simple and comprehensive models are shown in Figure 4.

For methane-dominated planets like K2-18 b,  $\text{CH}_4$  can also be constrained to  $\lesssim 1$  dex; in the case of an ideal cloud-free atmosphere, these constraints can be as low as  $\sim 0.5$  dex, similar to the  $\text{H}_2\text{O}$  abundance. For the other planets in our sample, with lower  $\text{CH}_4$  abundance, we find that inferences from Pandora result in upper limits on the  $\text{CH}_4$  abundance in the atmosphere. Similarly, we find that Pandora will be able to place upper limits on the abundance of  $\text{NH}_3$ . Finally, we find that for our targets, Pandora can successfully constrain the atmospheric temperature with uncertainties of  $\sim 100$  K even for atmospheres with high cloud coverage (e.g., HAT-P-18 b). The  $\text{CH}_4$  and  $\text{NH}_3$  posterior distributions can be found in Appendix B (Figure B1).

The constraints on atmospheric composition may be related to the atmospheric metallicity, an indicator of solid accretion during planet formation (e.g., C. Morasini et al. 2016). We find that Pandora will be able to provide constraints on the atmospheric metallicity with uncertainties of  $\lesssim 1$  dex with ten transit observations, making population-level analysis (e.g., L. Welbanks et al. 2019) with Pandora observations possible.

### 3.1.2. Scattering Slopes

We additionally consider the constraints on scattering slopes in the atmospheres of our target planets. Rayleigh scattering predominantly impacts bluer wavelengths ( $\lesssim 1 \mu\text{m}$ ), with a dependence on wavelength, scaling as  $\lambda^\gamma$ , where  $\gamma = -4$  for pure  $\text{H}_2$  Rayleigh scattering. Characterizing these slopes is crucial, as they both provide a baseline for the transit depth that ensures accurate measurements of absorption features (B. Benneke & S. Seager 2012) and contain information about aerosols (e.g., H. R. Wakeford & D. K. Sing 2015; A. Pinhas & N. Madhusudhan 2017). However, the shortwave predominance of scattering slopes makes them difficult to characterize with NIR instruments only. Scattering slopes can be enhanced by condensates and hazes (e.g., K. Ohno & Y. Kawashima 2020) but are broadly degenerate with the TLS effect (e.g., P. R. McCullough et al. 2014; N. Espinoza et al. 2019; A. Pinhas et al. 2018). Here, we consider two target cases with known Rayleigh or super-Rayleigh scattering (HD 189733 b and K2-18 b) and constraints with Pandora/NIRDA observations.

We find that in ten transits, observations with NIRDA will likely be sufficient to partially characterize the slope and amplitude enhancement of HD 189733 b’s scattering slope, providing accurate ( $< 1\sigma$ ) constraints on the amplitude enhancement and slope, with precisions of  $\sim 3$  dex and 5 respectively. However, we note that this slope may exhibit a degeneracy with the K abundance when only using NIRDA observations, due to the K

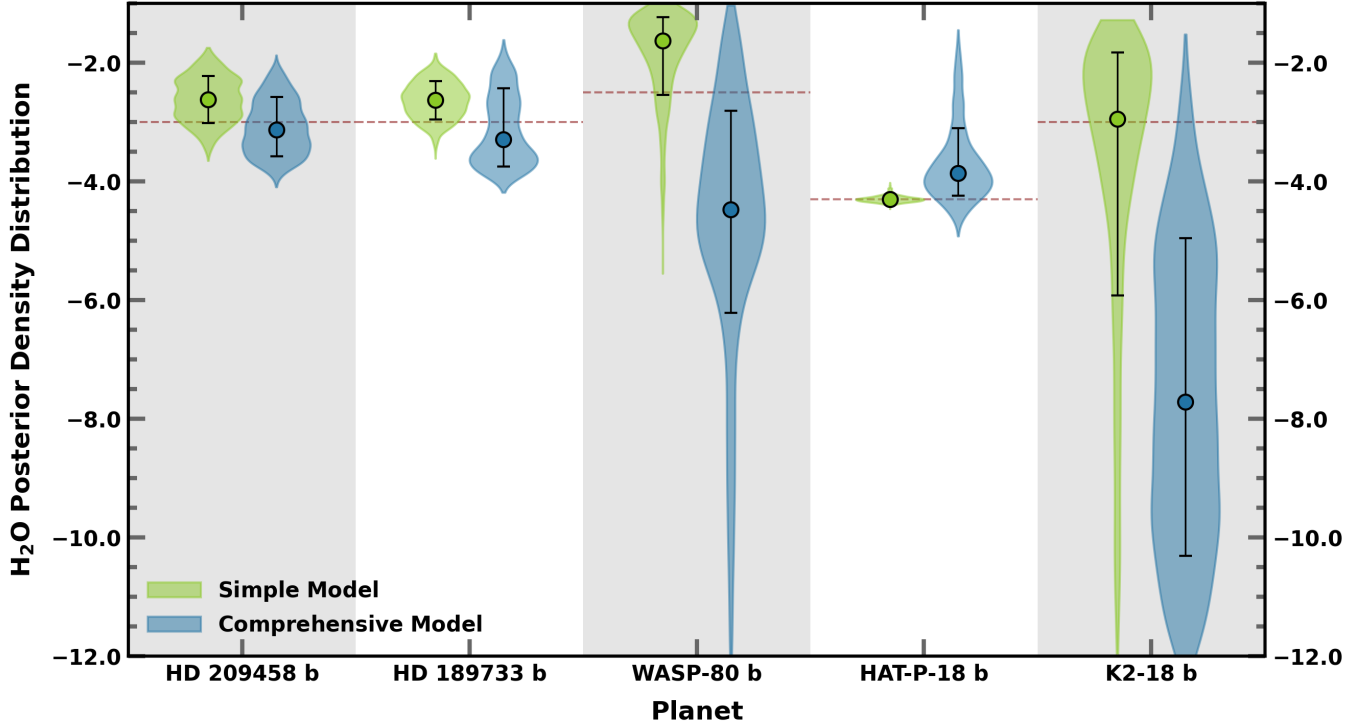


**Figure 4.**  $\text{H}_2\text{O}$  posterior distributions for our five targets. The green distributions show the retrieved posteriors from the simple model, and the blue represents the comprehensive model, which includes clouds and hazes (both described in Section 2.2). Maroon lines indicate the injected true values from Table 2 in Appendix A, and the error bars represent the 16th to 84th percentile range. While the simple model is able to accurately retrieve the  $\text{H}_2\text{O}$  abundance with high precision, the inclusion of clouds and hazes leads to degeneracies with the  $\text{H}_2\text{O}$  abundance (e.g., B. Benneke & S. Seager 2013; L. Welbanks & N. Madhusudhan 2019), making it more difficult to constrain  $\text{H}_2\text{O}$  with the realistic model.

doublet peaking at  $\sim 0.77 \mu\text{m}$ , off the blue edge of the NIRDA detector. A similar degeneracy has been noted in JWST/NIRISS observations, where the  $0.6 \mu\text{m}$  cutoff leads to observations of only the red wing of the Na doublet at  $\sim 0.59 \mu\text{m}$  (e.g., J. Taylor et al. 2023). Though we consider additional constraints provided by adding photometric data from Pandora/VISDA outside the scope of this work, leveraging such instruments may be instrumental in breaking this degeneracy for planets with strong optical slopes.

The analysis of K2-18 b results in constraints on the scattering enhancement amplitude and slope with precisions of 1.8 dex and 2.3, respectively. In order to identify the parameter space where aerosol scattering slopes will be constrainable with Pandora observations, we simulate new observations for K2-18 b, leaving all parameters constant aside from the enhancement factor, which we vary from 1 to  $10^{10}$ . For each of these, we simulate ten instances of observations to estimate the precision of the parameter posterior. We find that enhancements of  $\gtrsim 10^6$  will be observable using Pandora/NIRDA (Figure 5).

### 3.1.3. Identification of Chemical Absorbers

To analyze the ability of Pandora to identify the spectroscopic features of different chemical absorbers, we perform model comparisons between models that include or exclude a given absorber following the practices outlined in B. Benneke & S. Seager (2013) and further described in L. Welbanks & N. Madhusudhan (2021). The Bayes factor, i.e., the ratio of evidences between the two models, is a measure of the model preference, with a log-Bayes factor of  $|\ln B| > 5.0$  corresponding to strong significance at best (R. Trotta 2008). For the model described in Section 2.2 and under the assumptions of our synthetic observations, we find that Pandora can yield strong model preferences for the presence of  $\text{H}_2\text{O}$  — with values of  $\ln B$  ranging from  $-0.1$  for K2-18 b up to 544.3 for HD 209458 b. On the other hand,  $\text{CH}_4$  and  $\text{NH}_3$  absorption is not significantly preferred, e.g.,  $\ln B = 1.6$  for  $\text{CH}_4$  K2-18 b and  $\ln B < 0$  for  $\text{NH}_3$  in all five targets. These Bayesian model comparisons serve as an initial guideline for the capabilities of Pandora to identify spectral features and should be interpreted within the context of the atmospheric models considered as these comparisons do not represent unam-

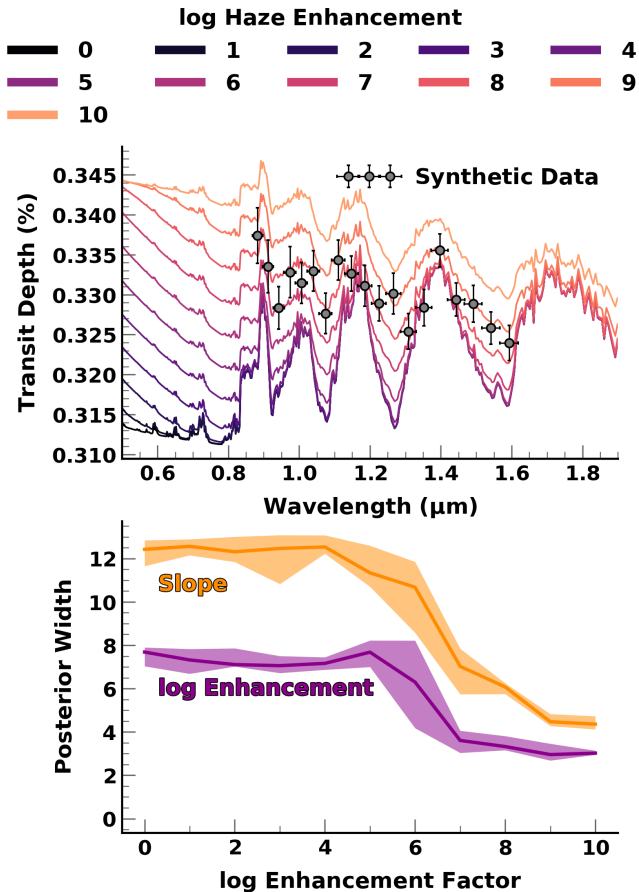


**Figure 5. Top:** The synthetic spectrum of K2-18 b overlaid with forward models with varying scattering slope enhancement amplitudes. Higher enhancement amplitudes affect the observed spectra further into the NIR, muting feature sizes in the  $\sim 1.0 \mu\text{m}$  range. **Bottom:** The 68% confidence interval of the posteriors of the enhancement ( $\log(a)$ ; purple) and slope ( $\gamma$ ; orange) for the different enhancements considered. At enhancements  $\gtrsim 10^6$ , the scattering slope more strongly affects the Pandora bandpass, allowing for more precise constraints on both parameters.

biguous chemical detections (see e.g., [L. Welbanks et al. 2023, 2025](#)).

### 3.2. Multi-Transit Observations

Alongside observations of the 20 primary mission targets, Pandora will be executing auxiliary target observations for targets of interest. It is therefore prudent to identify the number of transits that would need to be observed with Pandora for suitable constraints on a given target. Here we compare constraints on key atmospheric parameters for observations simulated for multiple transits, ranging from a single transit to 20 transits. We use the same simple HD 209458 b forward model as those in Section 3.1, limiting the absorbers to  $\text{H}_2\text{O}$ ,  $\text{CH}_4$ , and  $\text{NH}_3$ , as others will be unconstrained from Pandora

alone, and a cloud/haze free atmosphere. For each transit, we assume that the uncertainty in the observations can be scaled as  $1/\sqrt{N}$ , where  $N$  is the number of transits observed.

The constraints provided by Pandora observations improve with an increasing number of transits observed, particularly for the water abundance. The comparison of this for HD 209458 b is shown in Figure 6. Combining transits yields diminishing returns as  $N$  increases; going from 1 to 10 transit observations improves the  $\text{H}_2\text{O}$  posterior precision by a factor of  $\sim 2$ , but 10 and 20 transit observations provide roughly the same posterior width.

### 3.3. Observational Limits for Planetary Signals

The uncertainty in the planetary transit depth increases as a function of the stellar magnitude, making observations of planets even more challenging around fainter stars. Given this challenge and the range of magnitudes in Pandora’s primary target selection criteria ( $m_J$  between 7 and 11.5), we aim to determine the limit at which atmospheric spectra will be distinguishable from a flat spectrum.

We investigate these limits for observations of Jupiter-, Saturn-, and Neptune-sized archetypes (modeling these after HD 209458 b, WASP-80 b, and K2-18 b). For each target, we simulate observations of spectra across the range of Pandora’s stellar magnitude limits, normalizing to a 5-hour observation time for each transit. We consider 200 possible observations across the magnitude range for each target, with 100 noise instances at each magnitude. For each of these simulated observations, we use a chi-squared rejection test to calculate the probability of rejecting a flat line model. A rejection (e.g.,  $>3\sigma$ ) of a flat line implies a detection of an atmospheric signal. The results of these simulations are shown in Figure 7.

Largely, for target planets with stellar hosts of  $m_J \gtrsim 10$ , we find that distinguishing between an atmospheric signal and a flat line will require over ten transits, even for high-SNR targets. For smaller planets, a brighter host star is needed for a  $3\sigma$  atmospheric detection ( $m_J \lesssim 7.5$ ).

### 3.4. Identifying $\text{H}_2\text{O}$ Features with Pandora

For many smaller targets, a major hindrance in HST and JWST observations has been the disentanglement of stellar contamination from the planetary spectrum (e.g., [Z. Zhang et al. 2018](#); [H. R. Wakeford et al. 2019](#); [L. J. Garcia et al. 2022](#); [O. Lim et al. 2023](#); [S. E. Moran et al. 2023](#); [A. Banerjee et al. 2024](#); [N. Espinoza et al. 2025](#); [M. Radica et al. 2025](#); [A. D. Rathcke et al. 2025](#)). Pandora’s unique capability to constrain the stellar and

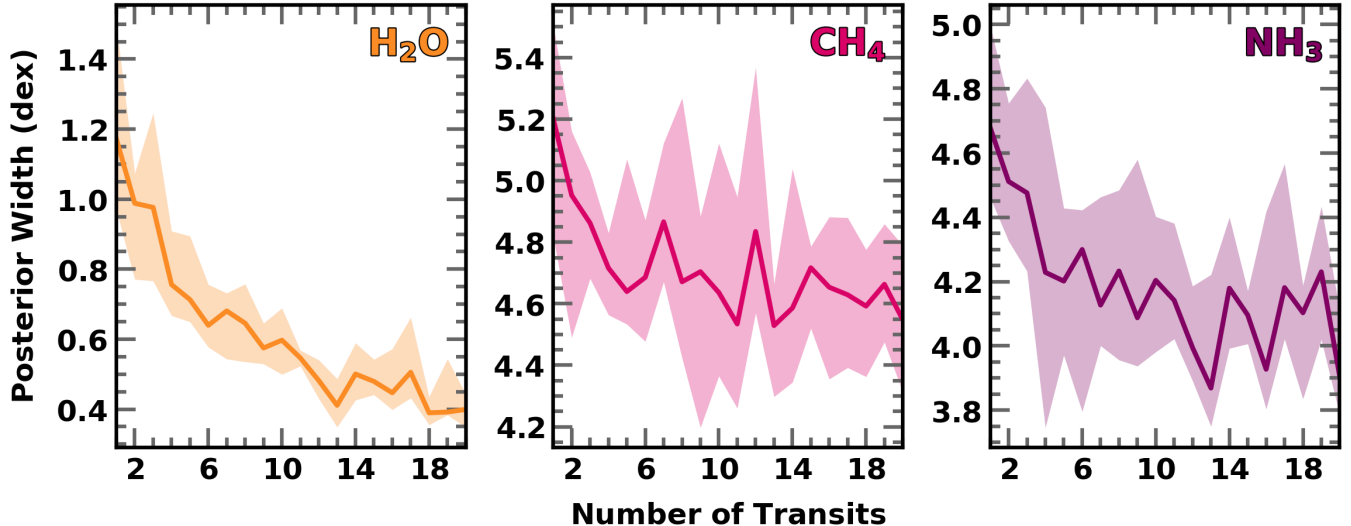


**Figure 6.** The width of the posterior (16<sup>th</sup> to 84<sup>th</sup> percentile) of the H<sub>2</sub>O, CH<sub>4</sub>, and NH<sub>3</sub> abundance for HD 209458 b as more transits are observed. The asymptotic nature of adding more transits can be clearly observed in the H<sub>2</sub>O posterior; adding ten transits leads to a reduction of  $\sim 50\%$  in the H<sub>2</sub>O posterior width for HD 209458 b, but there is a dropoff in relative improvement as  $N_{\text{trans}}$  becomes larger. CH<sub>4</sub> and NH<sub>3</sub> show some signs of tighter constraints when the number of transit observations is increased, but are more poorly constrained for HD 209458 b.

planetary spectra simultaneously and minimize the impact of stellar contamination presents a promising avenue for characterizing planets with ambiguous detections or no previous observations. We explore Pandora’s ability to determine the presence of an atmosphere (or a deviation from a flat line transmission spectrum) via the H<sub>2</sub>O absorption feature for each of our different planetary archetypes.

We first analytically calculate the expected signal-to-noise ratio (SNR) of a fully saturated H<sub>2</sub>O absorption feature in the atmosphere of each of our planets, in order to identify a first-order approximation for the signal strength of the 1.4  $\mu\text{m}$  water band. A fully saturated feature in a clear atmosphere covers about five scale heights in transit depth space (T. M. Brown 2001). Following this, we calculate the expected transit depth signal of a fully saturated feature given the scale height of each of our planets. We then calculate the minimum and maximum uncertainty in the Pandora H<sub>2</sub>O absorption band for each planet, and divide the two to calculate the expected range of SNRs of the water feature. We repeat this for a variety of stellar magnitudes.

Figure 8 shows the expected SNR for all five of our targets, with values of  $> 5$  implying a strongly detectable feature. We find that Pandora will be able to provide SNRs of  $> 5$  for clear atmospheres of targets around stars brighter than  $m_J \approx 10$ . In particular, low-density planets with hot atmospheres and bright hosts can allow for SNRs of up to  $\approx 75$ .

#### 4. COMBINING JWST AND PANDORA OBSERVATIONS

The launch of Pandora in January of 2026 coincides well with JWST, which is now over halfway finished with its nominal 5-year primary mission lifetime. JWST provides a broader wavelength range and higher precision than either HST or Pandora, making it capable of constraining the abundances of multiple carbon- and sulfur-bearing molecules (e.g., JWST Transiting Exoplanet Community Early Release Science Team et al. 2022; T. J. Bell et al. 2023). Here we compare inferences from JWST observations alone to those from combined Pandora and JWST observations of the same target. For each target, we simulate observations of a single transit with JWST/NIRCam, using the F322W2 and F444W filters, as well as for ten transits with Pandora, as described in Section 2. Because we aim to explore the consistency of Pandora across the parameter space of possible targets instead of its capability, we model each planet assuming an atmosphere in chemical equilibrium at a  $10\times$  solar metallicity, focusing on major carbon- and oxygen-bearing molecules (Section 2.2). We assume an aerosol-free atmosphere at the equilibrium temperature of each target. We run three retrievals for each case: one with only the simulated Pandora observations, one with only simulated JWST observations, and one with both. For these optimistic scenarios, we analyze the ability to provide accurate constraints on the atmospheric enrichment, defined here as  $(\text{C}+\text{O})/\text{H}$ .

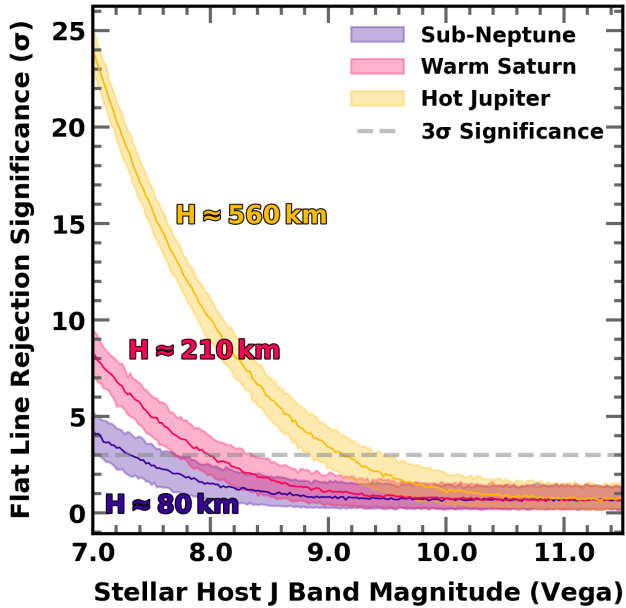


**Figure 7.** The rejection significance of a flat line for a hot Jupiter (HD 209458, yellow), warm Saturn (WASP-80, red), or sub-Neptune (K2-18, purple) at a given J band magnitude. For each planet, we model the transit depth uncertainty assuming ten observations of five hours. The ability to reject a flat line is a function of the atmospheric scale height (labeled as  $H$ ) versus the transit depth uncertainty. We show the  $3\sigma$  cutoff of a strong detection as a dashed gray line. For each planet, we show the median rejection significance and 68% confidence interval from 100 random noise realizations. As the host star gets fainter, the ability to distinguish between a flat line and an atmospheric signal decreases. For stars with  $m_J \gtrsim 10$ , most exoplanetary atmospheres will be require more than ten transits to distinguish from a featureless spectrum.

We find that the combination of Pandora and JWST observations largely provides better constraints (e.g., higher accuracy, precision, or both) than either the Pandora-only or JWST-only analysis. The inclusion of Pandora provides a valuable baseline for the transit depth and extends the wavelength coverage of JWST’s long-wavelength NIRCcam observations (section 4.1). The posterior distributions for the (C+O)/H measurements for all five targets, normalized to their solar expectations (J. I. Moses et al. 2013), are shown in Figure 9. Similar posteriors for individual species constrained in the retrieval can be found in Appendix C. While Pandora excels at inferring the oxygen abundance (via  $\text{H}_2\text{O}$ , the dominant oxygen-carrying species), it is less able to accurately constrain carbon (via CO and  $\text{CO}_2$ ), which is provided by the JWST observations.

Despite not having any strong absorption bands of CO or  $\text{CO}_2$ , we find that the inclusion of Pandora data may

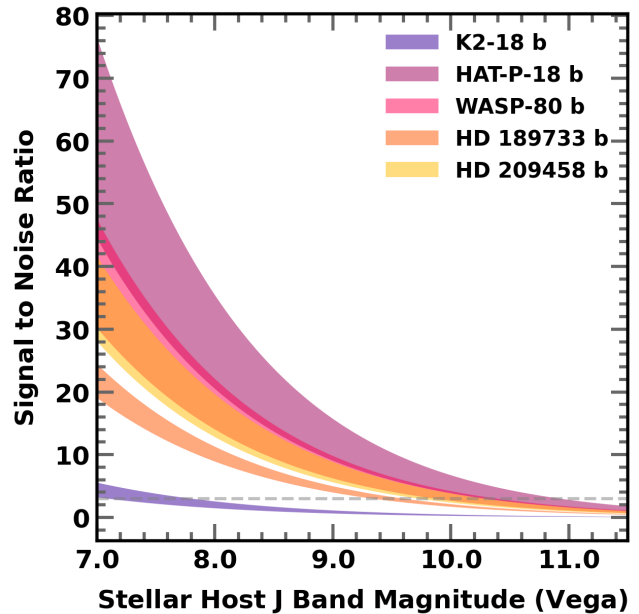


**Figure 8.** Estimated signal-to-noise ratios of the  $1.4 \mu\text{m}$   $\text{H}_2\text{O}$  absorption feature for each of our five targets at a given J band magnitude. For each planet, we model the transit depth uncertainty assuming ten observations of five hours. The cutoff for a signal ( $SNR = 3$ ) is shown with a gray dotted line. The bands represent the maximum and minimum SNRs given the range of uncertainties in bins covering the absorption feature. As the host star becomes fainter, the uncertainty increases and the SNR of the absorption feature becomes smaller. For bright targets ( $m_J \lesssim 10$ ) Pandora will be able to produce SNRs of 10–80 for clear atmospheres with saturated water absorption features.

help improve the constraints on both species when combined with JWST. Notably, for both HD 209458 b and HD 189733 b, which have the two highest CO abundances in our considered targets (Figure C2), the inclusion of Pandora observations helps improve the precision of the inferred CO abundance. Similarly, despite Pandora’s lack of  $\text{CO}_2$  constraints, all targets with  $\text{CO}_2$  except WASP-80 b show an improvement in the precision, accuracy, or both when Pandora is added to JWST/NIRCcam observations. This improvement is likely due to Pandora observations providing a larger baseline for the transit depth, enabling a better estimate of the spectral continuum (e.g., B. Benneke & S. Seager 2012).

#### 4.1. On the Importance of Optical and Near-IR Data from Pandora

To sufficiently characterize the atmosphere, observations in the optical and near-IR are often needed to complement data further towards the mid-IR wavelengths (e.g., H. R. Wakeford et al. 2018; C. Fairman et al. 2024).

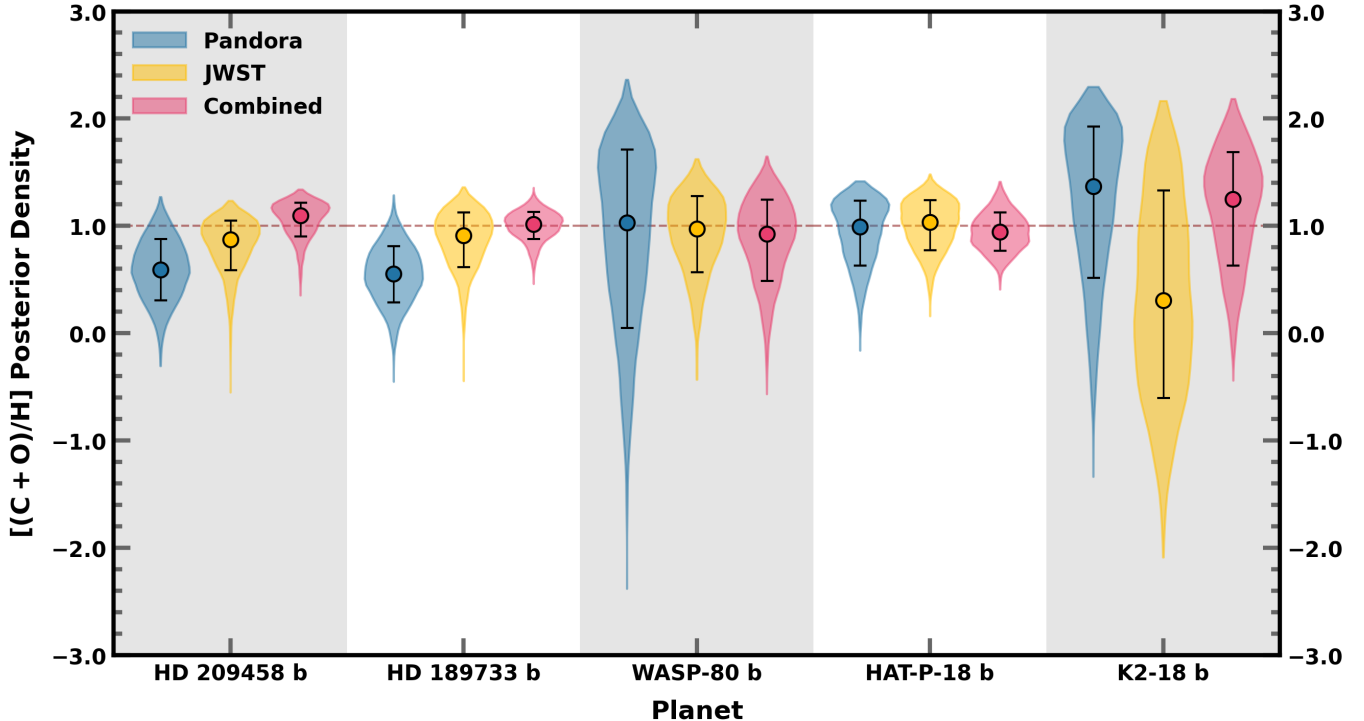


**Figure 9.** The posterior distributions of the metallicity (C+O/H) for each of our five targets inferred from Pandora, JWST, or combined observations. Metallicities are shown in logarithmic space and normalized to solar (e.g.,  $(C+O/H)_{\odot} = 0$ ). Blue histograms represent the constraints from Pandora data only, with yellow representing the JWST-only and red representing the combined JWST and Pandora cases. Maroon lines indicate the true value of the models ( $10\times$  solar), and the error bars represent the 16th to 84th percentile range. The combination of Pandora and JWST observations generally provides the most accurate and precise inference of the overall metallicity.

This allows for a transit depth baseline to be set (e.g., [B. Benneke & S. Seager 2012](#)), breaking key degeneracies affecting transmission spectra ([L. Welbanks & N. Madhusudhan 2019](#)), which may otherwise lead to bimodal posterior distributions obtained with mid-IR observations alone (e.g., [E. Schlawin et al. 2018](#)). Pandora’s spectroscopic and photometric bandpasses can provide NIR spectra down to  $\sim 0.9 \mu\text{m}$  and photometric data at  $\sim 0.5 \mu\text{m}$ , while simultaneously observing the near-IR.

Here we explore synergies of joint observations with Pandora and JWST. Motivated by previous analyses showing the importance of optical data (e.g., [H. R. Wakeford et al. 2018](#)), we present an analysis of HD 209458 b with combined JWST and Pandora observations. We generate a spectrum of HD 209458 b, following Section 3 but only including  $\text{H}_2\text{O}$  and  $\text{CO}_2$ , alongside a gray cloud opacity that covers 70% of the terminator. We consider observations with Pandora, JWST, or the combination of both, and vary the number of transit observations with Pandora from one to twenty. We consider the additional observations with Pandora/VISDA outside the scope of this comparison, though we note that it would likely further improve con-

straints when compared to JWST or Pandora/NIRDA alone. For each scenario, we consider ten noise instances of the Pandora data, to ensure that any inferences are not skewed by statistical outliers.

We find that by combining observations with Pandora and NIRCcam we obtain more reliable inferences on the  $\text{H}_2\text{O}$  abundance of HD 209458 b. In Figure 10, we show the  $1\sigma$  width (16<sup>th</sup> to 84<sup>th</sup> percentile range) of the  $\text{H}_2\text{O}$  abundance posteriors for each number of transits. Pandora observations by themselves have a larger  $1\sigma$  range ( $\sim 0.6$ – $1.4$  dex) than NIRCcam ( $\sim 0.4$ – $0.5$  dex); however, combining the observations allows for more precise constraints, down to  $\sim 0.3$  dex. In both cases, a plateau in the improvement is evident around the 10–12 transit mark, implying that for more than 12 transits, Pandora observations provide diminishing returns with respect to the water abundance constraint.

## 5. DISCUSSION AND SUMMARY

The upcoming Pandora SmallSat Mission is a dedicated exoplanet observatory, which presents a unique opportunity to study novel or complex systems and complement spectroscopic observations with other facilities, such as HST and JWST. In this work, we simulated

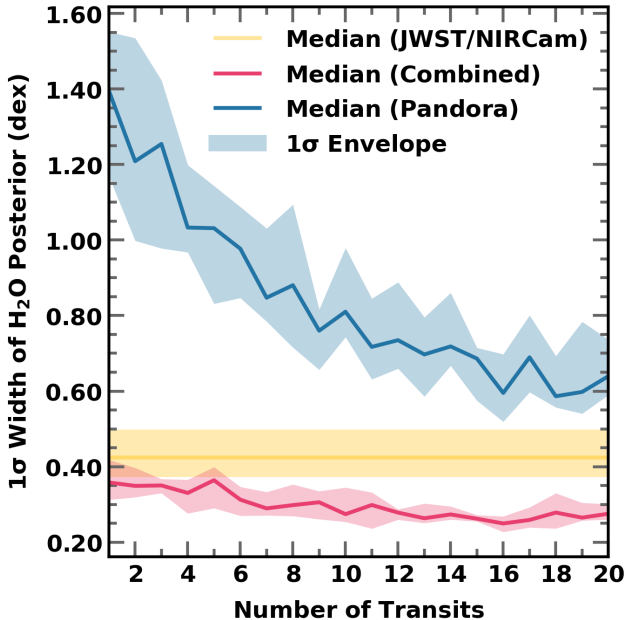


**Figure 10.** The width of posterior distributions of  $\text{H}_2\text{O}$  retrieved from synthetic observations of HD 209458 b. Inferences from Pandora observations are shown in light blue, with JWST/NIRCam/F322W+F444W in yellow. The inferences from combined observations of Pandora and NIRCam are shown in red. For each, we show the median and 68% confidence interval of the posterior width for each number of Pandora transits. By combining both datasets, the inferences can provide better precision on the water abundance than either instrument alone due to the additional wavelength coverage.

Pandora observations for five exoplanet targets, and analyzed the inferences that can be obtained from Pandora spectra, as well as combined Pandora and JWST spectra. We aimed to characterize Pandora’s capabilities for exoplanet targets and as a tool for improving JWST observations of planets around active stars. Here, we summarize our main findings in this work.

### 5.1. Detecting Atmospheric Signals

For bright targets ( $m_J \approx 7$ ), Pandora will be able to obtain spectra with precisions of 30–100 ppm after multiple transit observations. These precisions rival those of spectra obtained with HST’s WFC/G141 grism, a crucial instrument for constraining water abundances in exoplanet atmospheres for over a decade (e.g., D. Deming et al. 2013; L. Kreidberg et al. 2015; D. K. Sing et al. 2016). These precisions will allow for meaningful detections of an atmospheric signal (rejecting a flat line “no atmosphere” case at  $> 3\sigma$  confidence) for planets as small as sub-Neptunes, provided their host star is sufficiently bright and their atmospheres are aerosol-free and low-metallicity enough to provide large absorption

features. However, for host stars with  $m_J \gtrsim 10$ , the uncertainty for spectra obtained from ten stacked transits will be of order  $\sim 500$  ppm or higher. At those magnitudes, more than ten transit observations may be required to rule out flat spectra, even for those with large scale heights.

### 5.2. Constraining Atmospheric Spectra

With ten transits observed and stellar heterogeneity corrections, Pandora’s NIRDA spectra can constrain  $\text{H}_2\text{O}$  with precisions of  $\lesssim 1$  dex and atmospheric temperatures to within  $\lesssim 100$  K for the scenarios considered here. Pandora will also be able to observe the  $1.4 \mu\text{m}$   $\text{H}_2\text{O}$  absorption feature with a signal-to-noise ratio of up to  $SNR = 75$  for fully saturated, cloud-free atmospheres. Additionally, Pandora has the potential to place accurate upper limits on the abundance of  $\text{CH}_4$  and  $\text{NH}_3$  in exoplanet atmospheres, and may be able to provide constraints of  $\approx 1$  dex on the  $\text{CH}_4$  abundance for methane-dominated atmospheres of sub-Neptunes (e.g., K2-18 b; N. Madhusudhan et al. 2023). The latter will depend on the capability to distinguish between  $\text{CH}_4$  and  $\text{H}_2\text{O}$  absorption, which has presented an issue for previous observations with HST/WFC3 G141 (e.g., M. M. Murphy et al. 2025). This, however, may be overcome with observations of  $\text{CH}_4$  absorption at longer wavelengths with JWST (e.g., T. J. Bell et al. 2023; L. Welbanks et al. 2024), presenting a key synergistic avenue between the two telescopes. Additionally, constraints on the chemical inventory of the planetary atmosphere from Pandora observations alone may allow for accurate constraints of  $\lesssim 1.3$  dex on the atmospheric metallicity for atmospheres with large absorption features, allowing for population-level analysis of the bulk composition. We note that, particularly for sub-Neptunes, this is dependent on the atmospheric temperature, metallicity, and aerosol content of the atmosphere, as they may have high-metallicity or aerosol-obscured atmospheres indistinguishable with JWST from atmospheric non-detections (e.g., N. L. Wallock et al. 2024; E. Schlawin et al. 2024).

Furthermore, observations with Pandora/NIRDA may be able to place constraints on the scattering slope for particularly hazy planets. Rayleigh scattering slopes in transmission spectra are often enhanced by haze scattering in the upper atmosphere (e.g., A. Lecavelier des Etangs et al. 2008; F. Pont et al. 2013), leading to large slopes in optical wavelengths that may extend out towards NIR absorption features. Constraining this slope is crucial for analysis of the transmission spectrum. Firstly, the angle and enhancement of the slope provide key information about haze composition in the

atmosphere (e.g., A. Pinhas & N. Madhusudhan 2017; K. Ohno & Y. Kawashima 2020). Secondly, it provides a key measurement of the mean molecular weight of the atmosphere (B. Benneke & S. Seager 2012), allowing for disentanglement of the degeneracy between temperature and mean molecular weight that arises from only measuring the scale height via absorption features (e.g., L. Welbanks & N. Madhusudhan 2019). Most importantly, the scattering slope is often degenerate with TLS features, which preferentially affect shorter wavelengths (e.g., B. V. Rackham et al. 2019; A. R. Iyer & M. R. Line 2020). This can lead to artificially large super-Rayleigh slopes (e.g., C. I. Cañas et al. 2025) or negative slopes (e.g., C. Cadieux et al. 2024). Pandora may be able to constrain haze scattering slopes and enhancement factors for Rayleigh scattering with enhancements of more than  $\sim 10^6$ . We note that we do not consider the effects of uncorrected TLS features in our spectra, and the ability to simultaneously constrain stellar and planetary properties; a companion study (B. V. Rackham et al. 2026) explores Pandora’s constraining capabilities for the host stars and its impacts at the data and model levels.

### 5.3. Synergy with JWST

We further consider the synergies of Pandora and JWST when observing absorption features in the planetary spectrum. Combining Pandora and JWST observations can provide constraints on molecular abundances, particularly  $\text{H}_2\text{O}$ , that are both more precise and more accurate than achievable with either telescope separately (Figure 9). The inclusion of Pandora provides a valuable wavelength baseline for observations at longer wavelengths with JWST (e.g., NIRCam), as well as an independent measurement of the water absorption feature, allowing for relative feature sizes in the JWST observations to be converted into absolute abundance measurements. This improvement with the addition of lower-wavelength data has been previously noted for HST (e.g., C. Fairman et al. 2024) and JWST; for example, N. E. Batalha & M. R. Line (2017) noted the preference for broadband observations over repeated observations when aiming for accurate inferences from the planetary atmosphere.

Furthermore, we find that the inclusion of Pandora observations can help improve constraints on gases not accessible with Pandora alone, such as  $\text{CO}_2$  (Figure C2). Although Pandora can only place upper limits on the  $\text{CO}_2$  abundance by itself, the wavelength coverage of Pandora provides a key baseline for comparing to the  $\text{CO}_2$  feature observed with JWST. As such, we find that the  $\text{CO}_2$  constraints acquired from joint JWST and Pan-

dora observations can be both more precise and more accurate than achievable with JWST alone.

We further explore the effect of multiple Pandora transit observations in combination with JWST. We find that combining multiple Pandora transits will provide more precise inferences of absorber abundances, though the effect of increasing the number of observations is lessened for absorbers with only upper limit characterization. In particular, the improvement due to an increased number of transits is most effective up until  $\sim 10$ – $12$  transits, after which the precision does not improve significantly. Moreover, we find that the combination of Pandora observations with JWST will provide more precise inferences than possible with either instrument alone (leading to inferences as precise as  $\sim 0.25$  dex with the combined instrumentation at 10 transits).

### 5.4. Looking Forward with JWST and Pandora

With JWST now in operation for more than three years of exoplanet observations, the field of exoplanet science is accelerating at a rapid pace. At the forefront of the field are questions about planet formation and evolution, including the composition of small planet atmospheres and the effect of underlying star–planet connections on both our inferences and the planet itself. Often, active host stars present barriers for JWST observations of their planets, including disagreement across multiple observations or biased estimates of abundances (e.g., G. Fu et al. 2022; M. Fournier-Tondreau et al. 2024a). While modeling methodologies have been proposed to overcome unknowns introduced in the observations by stellar activity (e.g., Y. Rotman et al. 2025; N. Espinoza et al. 2025), an approach at the data level is needed to ensure reliable observations. Pandora is a mission designed specifically to better understand and overcome these challenges.

In addition to improved characterization of individual planet atmospheres, the combination of JWST and Pandora offers an opportunity to further the study of populations of planet atmospheres. A significant, growing body of work concerns the understanding of different classes of planet atmospheres, the processes that drive their evolution, and their relative frequencies (see, e.g. E. M. R. Kempton & H. A. Knutson 2024, and references therein). One roadblock to these analyses is the difficulty interpreting the depth of NIR spectral features in the absence of shorter wavelength information constraining the scattering slope. By providing these crucial complementary data for planets over a wide range of sizes and temperatures, Pandora will contribute significantly to population-level analyses of planets observed with JWST.

Alongside the opportunities explored throughout this work, Pandora provides a unique opportunity to help overcome many hurdles inherent in observations with current instruments. Namely, multi-epoch observations of exoplanet atmospheres with JWST are often observed at different points in the stellar rotation, making them difficult to fit jointly (e.g., [E. M. May et al. 2023](#)). By providing information about the stellar activity and allowing for corrections at the data level, joint Pandora–JWST programs will unlock new insights into planets around active hosts. Additionally, these same insights will inform the presence of offsets between different instruments and epochs, which have been difficult to constrain thus far with JWST alone (e.g., [A. L. Carter et al. 2024](#)).

Pandora presents a new opportunity to provide important constraints on the atmospheric composition, temperature, and metallicity of exoplanets, particularly in the presence of stellar activity. Furthermore, SmallSats like Pandora provide important avenues for synergizing with current flagship missions. Leveraging Pandora’s capabilities and synergies with JWST over its 1 year prime mission will help ensure that we maximize the science information available to us both now and over the coming decades of exoplanet science.

#### ACKNOWLEDGMENTS

The authors would like to thank the reviewer for the comments that significantly improved the manuscript. Pandora is supported by NASA’s Astrophysics Pioneers Program. This work was performed under the auspices of the U.S. Department of Energy by Lawrence Livermore National Laboratory under Contract DE-AC52-07NA27344. The document number is LLNL-JRNL-2009856. Y.R. and P.M. were supported under

the LLNL Space Science Institute’s Institutional Scientific Capability Portfolio. Computing support for this work came from the Lawrence Livermore National Laboratory 19th Institutional Computing Grand Challenge program. L.W. and Y.R. acknowledge support from NASA XRP Grant [80NSSC24K0160]. L.W. thanks the Heising-Simons Foundation for support under the 51 Pegasus b Fellowship. This material is based upon work supported by NASA under award No. 80NSSC24K0197. This material is partly based upon work supported by the National Aeronautics and Space Administration under Agreement No. 80NSSC21K0593 for the program “Alien Earths”. The results reported herein benefited from collaborations and/or information exchange within NASA’s Nexus for Exoplanet System Science (NExSS) research coordination network sponsored by NASA’s Science Mission Directorate. This material is based upon work supported by the European Research Council (ERC) Synergy Grant under the European Union’s Horizon 2020 research and innovation program (grant No. 101118581—project REVEAL). T.G. acknowledges NASA Pandora funding through WBS 344310.01.02.01.02. B.J.H. acknowledges funding support from grant ORAU - 80HQTR21CA005. T.O.F. acknowledges funding support through the NASA Postdoctoral Program Grant Number: ORAU - 80HQTR21CA005. J.F.R. acknowledges financial support from the NSERC Discovery Program and the Canadian Space Agency ROSS program. K. H. acknowledges the support of the Canadian Space Agency (CSA) [22EXPRESS1].

*Software:* NumPy ([C. R. Harris et al. 2020](#)), AstroPy ([The Astropy Collaboration et al. 2022](#)), PandoraSat and PandoraSim ([C. Hedges et al. 2024](#)), Matplotlib ([J. D. Hunter 2007](#)), MultiNest ([F. Feroz et al. 2009](#)) via PyMultiNest ([J. Buchner et al. 2014](#)).

#### REFERENCES

- Addison, B., Wright, D. J., Wittenmyer, R. A., et al. 2019, *Publications of the Astronomical Society of the Pacific*, 131, 115003, doi: [10.1088/1538-3873/ab03aa](https://doi.org/10.1088/1538-3873/ab03aa)
- Agol, E., Cowan, N. B., Knutson, H. A., et al. 2010, *The Astrophysical Journal*, 721, 1861, doi: [10.1088/0004-637X/721/2/1861](https://doi.org/10.1088/0004-637X/721/2/1861)
- Allard, N. F., Spiegelman, F., & Kielkopf, J. F. 2016, *Astronomy and Astrophysics*, 589, A21, doi: [10.1051/0004-6361/201628270](https://doi.org/10.1051/0004-6361/201628270)
- Allard, N. F., Spiegelman, F., Leininger, T., & Molliere, P. 2019, *Astronomy and Astrophysics*, 628, A120, doi: [10.1051/0004-6361/201935593](https://doi.org/10.1051/0004-6361/201935593)
- Banerjee, A., Barstow, J. K., Gressier, A., et al. 2024, *The Astrophysical Journal Letters*, 975, L11, doi: [10.3847/2041-8213/ad73d0](https://doi.org/10.3847/2041-8213/ad73d0)
- Barclay, T., Quintana, E. V., Colón, K., et al. 2025, arXiv, doi: [10.48550/arXiv.2502.09730](https://doi.org/10.48550/arXiv.2502.09730)
- Batalha, N. E., & Line, M. R. 2017, *AJ*, 153, 151, doi: [10.3847/1538-3881/aa5faa](https://doi.org/10.3847/1538-3881/aa5faa)
- Batalha, N. E., Mandell, A., Pontoppidan, K., et al. 2017, *Publications of the Astronomical Society of the Pacific*, 129, 064501, doi: [10.1088/1538-3873/aa65b0](https://doi.org/10.1088/1538-3873/aa65b0)

- Beatty, T. G., Welbanks, L., Schlawin, E., et al. 2024, *The Astrophysical Journal*, 970, L10, doi: [10.3847/2041-8213/ad55e9](https://doi.org/10.3847/2041-8213/ad55e9)
- Bell, T. J., Welbanks, L., Schlawin, E., et al. 2023, *Nature*, 623, 709, doi: [10.1038/s41586-023-06687-0](https://doi.org/10.1038/s41586-023-06687-0)
- Benneke, B., & Seager, S. 2012, *The Astrophysical Journal*, 753, 100, doi: [10.1088/0004-637X/753/2/100](https://doi.org/10.1088/0004-637X/753/2/100)
- Benneke, B., & Seager, S. 2013, *The Astrophysical Journal*, 778, 153, doi: [10.1088/0004-637X/778/2/153](https://doi.org/10.1088/0004-637X/778/2/153)
- Benneke, B., Wong, I., Piaulet, C., et al. 2019, *The Astrophysical Journal Letters*, 887, L14, doi: [10.3847/2041-8213/ab59dc](https://doi.org/10.3847/2041-8213/ab59dc)
- Bouchy, F., Udry, S., Mayor, M., et al. 2005, *Astronomy and Astrophysics*, 444, L15, doi: [10.1051/0004-6361:200500201](https://doi.org/10.1051/0004-6361:200500201)
- Broggi, M., & Line, M. R. 2019, *The Astronomical Journal*, 157, 114, doi: [10.3847/1538-3881/aaffd3](https://doi.org/10.3847/1538-3881/aaffd3)
- Brown, T. M. 2001, *The Astrophysical Journal*, 553, 1006, doi: [10.1086/320950](https://doi.org/10.1086/320950)
- Buchner, J., Georgakakis, A., Nandra, K., et al. 2014, *Astronomy & Astrophysics*, 564, A125, doi: [10.1051/0004-6361/201322971](https://doi.org/10.1051/0004-6361/201322971)
- Cadieux, C., Doyon, R., MacDonald, R. J., et al. 2024, *The Astrophysical Journal*, 970, L2, doi: [10.3847/2041-8213/ad5afa](https://doi.org/10.3847/2041-8213/ad5afa)
- Carleo, I., Giacobbe, P., Guilluy, G., et al. 2022, *The Astronomical Journal*, 164, 101, doi: [10.3847/1538-3881/ac80bf](https://doi.org/10.3847/1538-3881/ac80bf)
- Carter, A. L., May, E. M., Espinoza, N., et al. 2024, *Nature Astronomy*, 8, 1008, doi: [10.1038/s41550-024-02292-x](https://doi.org/10.1038/s41550-024-02292-x)
- Cañas, C. I., Lustig-Yaeger, J., Tsai, S.-M., et al. 2025, arXiv, doi: [10.48550/arXiv.2502.06966](https://doi.org/10.48550/arXiv.2502.06966)
- Charbonneau, D., Brown, T. M., Latham, D. W., & Mayor, M. 2000, *The Astrophysical Journal*, 529, L45, doi: [10.1086/312457](https://doi.org/10.1086/312457)
- Charbonneau, D., Brown, T. M., Noyes, R. W., & Gilliland, R. L. 2002, *The Astrophysical Journal*, 568, 377, doi: [10.1086/338770](https://doi.org/10.1086/338770)
- Charbonneau, D., Knutson, H. A., Barman, T., et al. 2008, *The Astrophysical Journal*, 686, 1341, doi: [10.1086/591635](https://doi.org/10.1086/591635)
- Cloutier, R., Astudillo-Defru, N., Doyon, R., et al. 2019, *Astronomy & Astrophysics*, 621, A49, doi: [10.1051/0004-6361/201833995](https://doi.org/10.1051/0004-6361/201833995)
- Deming, D., Wilkins, A., McCullough, P., et al. 2013, *The Astrophysical Journal*, 774, 95, doi: [10.1088/0004-637X/774/2/95](https://doi.org/10.1088/0004-637X/774/2/95)
- Dyrek, A., Min, M., Decin, L., et al. 2024, *Nature*, 625, 51, doi: [10.1038/s41586-023-06849-0](https://doi.org/10.1038/s41586-023-06849-0)
- Espinoza, N., & Perrin, M. D. 2025, arXiv, doi: [10.48550/arXiv.2505.20520](https://doi.org/10.48550/arXiv.2505.20520)
- Espinoza, N., Rackham, B. V., Jordán, A., et al. 2019, *MNRAS*, 482, 2065, doi: [10.1093/mnras/sty2691](https://doi.org/10.1093/mnras/sty2691)
- Espinoza, N., Allen, N. H., Glidden, A., et al. 2025, *ApJL*, 990, L52, doi: [10.3847/2041-8213/adf42e](https://doi.org/10.3847/2041-8213/adf42e)
- Evans, T. M., Aigrain, S., Gibson, N., et al. 2015, *Monthly Notices of the Royal Astronomical Society*, 451, 680, doi: [10.1093/mnras/stv910](https://doi.org/10.1093/mnras/stv910)
- Fairman, C., Wakeford, H. R., & MacDonald, R. J. 2024, arXiv. <https://arxiv.org/abs/2403.07801>
- Feroz, F., Hobson, M. P., & Bridges, M. 2009, *Monthly Notices of the Royal Astronomical Society*, 398, 1601, doi: [10.1111/j.1365-2966.2009.14548.x](https://doi.org/10.1111/j.1365-2966.2009.14548.x)
- Foote, T. O., Quintana, E. V., Dotson, J. L., et al. 2022, in *Space Telescopes and Instrumentation 2022: Optical, Infrared, and Millimeter Wave*, Vol. 12180 (SPIE), 1060–1070, doi: [10.1117/12.2630131](https://doi.org/10.1117/12.2630131)
- Fournier-Tondreau, M., MacDonald, R. J., Radica, M., et al. 2024a, *Monthly Notices of the Royal Astronomical Society*, 528, 3354, doi: [10.1093/mnras/stad3813](https://doi.org/10.1093/mnras/stad3813)
- Fournier-Tondreau, M., Pan, Y., Morel, K., et al. 2024b, arXiv, doi: [10.48550/arXiv.2412.17072](https://doi.org/10.48550/arXiv.2412.17072)
- Fu, G., Espinoza, N., Sing, D. K., et al. 2022, *The Astrophysical Journal Letters*, 940, L35, doi: [10.3847/2041-8213/ac9977](https://doi.org/10.3847/2041-8213/ac9977)
- Fu, G., Welbanks, L., Deming, D., et al. 2024, *Nature*, Volume 632, Issue 8026, pp. 752–756, 632, 752, doi: [10.1038/s41586-024-07760-y](https://doi.org/10.1038/s41586-024-07760-y)
- Fukui, A., Kawashima, Y., Ikoma, M., et al. 2014, *The Astrophysical Journal*, 790, 108, doi: [10.1088/0004-637X/790/2/108](https://doi.org/10.1088/0004-637X/790/2/108)
- Garcia, L. J., Moran, S. E., Rackham, B. V., et al. 2022, *A&A*, 665, A19, doi: [10.1051/0004-6361/202142603](https://doi.org/10.1051/0004-6361/202142603)
- Gardner, J. P., Mather, J. C., Clampin, M., et al. 2006, *Space Science Reviews*, 123, 485, doi: [10.1007/s11214-006-8315-7](https://doi.org/10.1007/s11214-006-8315-7)
- Giacobbe, P., Brogi, M., Gandhi, S., et al. 2021, *Nature*, 592, 205, doi: [10.1038/s41586-021-03381-x](https://doi.org/10.1038/s41586-021-03381-x)
- Greene, T. P., Line, M. R., Montero, C., et al. 2016, *The Astrophysical Journal*, 817, 17, doi: [10.3847/0004-637X/817/1/17](https://doi.org/10.3847/0004-637X/817/1/17)
- Harris, C. R., Millman, K. J., van der Walt, S. J., et al. 2020, *Nature*, 585, 357, doi: [10.1038/s41586-020-2649-2](https://doi.org/10.1038/s41586-020-2649-2)
- Hartman, J. D., Bakos, G. A., Sato, B., et al. 2010, *The Astrophysical Journal*, 726, 52, doi: [10.1088/0004-637X/726/1/52](https://doi.org/10.1088/0004-637X/726/1/52)
- Hedges, C., Holcomb, R. J., Hord, B., et al. 2024, in *Software and Cyberinfrastructure for Astronomy VIII*, Vol. 13101 (SPIE), 182–190, doi: [10.1117/12.3020326](https://doi.org/10.1117/12.3020326)

- Hoffman, K., Quintana, E. V., Dotson, J. L., et al. 2022, in *Space Telescopes and Instrumentation 2022: Optical, Infrared, and Millimeter Wave*, Vol. 12180 (SPIE), 80–88, doi: [10.1117/12.2629546](https://doi.org/10.1117/12.2629546)
- Hu, R., Bello-Arufe, A., Tokadjian, A., et al. 2025, arXiv, doi: [10.48550/arXiv.2507.12622](https://doi.org/10.48550/arXiv.2507.12622)
- Hunter, J. D. 2007, *Computing in Science & Engineering*, 9, 90, doi: [10.1109/MCSE.2007.55](https://doi.org/10.1109/MCSE.2007.55)
- Husser, T. O., Wende-von Berg, S., Dreizler, S., et al. 2013, *Astronomy and Astrophysics*, 553, A6, doi: [10.1051/0004-6361/201219058](https://doi.org/10.1051/0004-6361/201219058)
- Inglis, J., Batalha, N. E., Lewis, N. K., et al. 2024, doi: [10.3847/2041-8213/ad725e](https://doi.org/10.3847/2041-8213/ad725e)
- Iyer, A. R., & Line, M. R. 2020, *The Astrophysical Journal*, 889, 78, doi: [10.3847/1538-4357/ab612e](https://doi.org/10.3847/1538-4357/ab612e)
- Jacobs, B., Désert, J.-M., Gao, P., et al. 2023, *The Astrophysical Journal*, 956, L43, doi: [10.3847/2041-8213/acfee9](https://doi.org/10.3847/2041-8213/acfee9)
- JWST Transiting Exoplanet Community Early Release Science Team, Ahrer, E.-M., Alderson, L., et al. 2022, arXiv, doi: [10.48550/arXiv.2208.11692](https://doi.org/10.48550/arXiv.2208.11692)
- Kempton, E. M. R., & Knutson, H. A. 2024, *Reviews in Mineralogy and Geochemistry*, 90, 411, doi: [10.2138/rmg.2024.90.12](https://doi.org/10.2138/rmg.2024.90.12)
- Kirk, J., Wheatley, P. J., Loudon, T., et al. 2017, *Monthly Notices of the Royal Astronomical Society*, 468, 3907, doi: [10.1093/mnras/stx752](https://doi.org/10.1093/mnras/stx752)
- Kreidberg, L., Line, M. R., Bean, J. L., et al. 2015, *The Astrophysical Journal*, 814, 66, doi: [10.1088/0004-637X/814/1/66](https://doi.org/10.1088/0004-637X/814/1/66)
- Lecavelier des Etangs, A., Pont, F., Vidal-Madjar, A., & Sing, D. 2008, *Astronomy & Astrophysics*, 481, L83, doi: [10.1051/0004-6361:200809388](https://doi.org/10.1051/0004-6361:200809388)
- Lim, O., Benneke, B., Doyon, R., et al. 2023, *The Astrophysical Journal Letters*, 955, L22, doi: [10.3847/2041-8213/acf7c4](https://doi.org/10.3847/2041-8213/acf7c4)
- Line, M. R., & Parmentier, V. 2016, *The Astrophysical Journal*, 820, 78, doi: [10.3847/0004-637X/820/1/78](https://doi.org/10.3847/0004-637X/820/1/78)
- Madhusudhan, N. 2012, *The Astrophysical Journal*, 758, 36, doi: [10.1088/0004-637X/758/1/36](https://doi.org/10.1088/0004-637X/758/1/36)
- Madhusudhan, N. 2018, in *Springer Handbook of Exoplanets*, 2153–2182, doi: [10.1007/978-3-319-55333-7\\_104](https://doi.org/10.1007/978-3-319-55333-7_104)
- Madhusudhan, N., Nixon, M. C., Welbanks, L., Piette, A. A., & Booth, R. A. 2020, *The Astrophysical Journal*, 891, L7, doi: [10.3847/2041-8213/ab7229](https://doi.org/10.3847/2041-8213/ab7229)
- Madhusudhan, N., Sarkar, S., Constantinou, S., et al. 2023, *The Astrophysical Journal*, 956, L13, doi: [10.3847/2041-8213/acf577](https://doi.org/10.3847/2041-8213/acf577)
- Madhusudhan, N., & Seager, S. 2009, *The Astrophysical Journal*, 707, 24, doi: [10.1088/0004-637X/707/1/24](https://doi.org/10.1088/0004-637X/707/1/24)
- Mancini, L., Southworth, J., Ciceri, S., et al. 2014, *Astronomy and Astrophysics*, 562, A126, doi: [10.1051/0004-6361/201323265](https://doi.org/10.1051/0004-6361/201323265)
- May, E. M., MacDonald, R. J., Bennett, K. A., et al. 2023, *The Astrophysical Journal Letters*, 959, L9, doi: [10.3847/2041-8213/ad054f](https://doi.org/10.3847/2041-8213/ad054f)
- McCullough, P. R., Crouzet, N., Deming, D., & Madhusudhan, N. 2014, *The Astrophysical Journal*, 791, 55, doi: [10.1088/0004-637X/791/1/55](https://doi.org/10.1088/0004-637X/791/1/55)
- Miller-Ricci, E., Rowe, J. F., Sasselov, D., et al. 2008, *The Astrophysical Journal*, 682, 593, doi: [10.1086/587634](https://doi.org/10.1086/587634)
- Montet, B. T., Morton, T. D., Foreman-Mackey, D., et al. 2015, *The Astrophysical Journal*, 809, 25, doi: [10.1088/0004-637X/809/1/25](https://doi.org/10.1088/0004-637X/809/1/25)
- Moran, S. E., Stevenson, K. B., Sing, D. K., et al. 2023, *The Astrophysical Journal Letters*, 948, L11, doi: [10.3847/2041-8213/accb9c](https://doi.org/10.3847/2041-8213/accb9c)
- Mordasini, C., Boekel, R. v., Mollière, P., Henning, T., & Benneke, B. 2016, *The Astrophysical Journal*, 832, 41, doi: [10.3847/0004-637X/832/1/41](https://doi.org/10.3847/0004-637X/832/1/41)
- Moses, J. I., Line, M. R., Visscher, C., et al. 2013, *ApJ*, 777, 34, doi: [10.1088/0004-637X/777/1/34](https://doi.org/10.1088/0004-637X/777/1/34)
- Muirhead, P. S., Dressing, C. D., Mann, A. W., et al. 2018, *The Astronomical Journal*, 155, 180, doi: [10.3847/1538-3881/aab710](https://doi.org/10.3847/1538-3881/aab710)
- Murphy, M. M., Beatty, T. G., Welbanks, L., & Fu, G. 2025, *The Astronomical Journal*, Volume 169, Issue 6, id.286, 19 pp., 169, 286, doi: [10.3847/1538-3881/adc684](https://doi.org/10.3847/1538-3881/adc684)
- Narrett, I. S., Rackham, B. V., & de Wit, J. 2024, *The Astronomical Journal*, 167, 107, doi: [10.3847/1538-3881/ad1ff6c](https://doi.org/10.3847/1538-3881/ad1ff6c)
- Ohno, K., & Kawashima, Y. 2020, *The Astrophysical Journal Letters*, 895, L47, doi: [10.3847/2041-8213/ab93d7](https://doi.org/10.3847/2041-8213/ab93d7)
- Pinhas, A., & Madhusudhan, N. 2017, *Monthly Notices of the Royal Astronomical Society*, 471, 4355, doi: [10.1093/mnras/stx1849](https://doi.org/10.1093/mnras/stx1849)
- Pinhas, A., Rackham, B. V., Madhusudhan, N., & Apai, D. 2018, *Monthly Notices of the Royal Astronomical Society*, 480, 5314, doi: [10.1093/mnras/sty2209](https://doi.org/10.1093/mnras/sty2209)
- Pont, F., Knutson, H., Gilliland, R. L., Moutou, C., & Charbonneau, D. 2008, *Monthly Notices of the Royal Astronomical Society*, 385, 109, doi: [10.1111/j.1365-2966.2008.12852.x](https://doi.org/10.1111/j.1365-2966.2008.12852.x)
- Pont, F., Sing, D. K., Gibson, N. P., et al. 2013, *Monthly Notices of the Royal Astronomical Society*, 432, 2917, doi: [10.1093/mnras/stt651](https://doi.org/10.1093/mnras/stt651)
- Quintana, E. V., Colón, K. D., Mosby, G., et al. 2021, arXiv, doi: [10.48550/arXiv.2108.06438](https://doi.org/10.48550/arXiv.2108.06438)

- Quintana, E. V., Dotson, J. L., Colón, K. D., et al. 2024, in *Space Telescopes and Instrumentation 2024: Optical, Infrared, and Millimeter Wave*, Vol. 13092 (SPIE), 359–367, doi: [10.1117/12.3020633](https://doi.org/10.1117/12.3020633)
- Rackham, B., Espinoza, N., Apai, D., et al. 2017, *ApJ*, 834, 151, doi: [10.3847/1538-4357/aa4f6c](https://doi.org/10.3847/1538-4357/aa4f6c)
- Rackham, B. V., Apai, D., & Giampapa, M. S. 2018, *ApJ*, 853, 122, doi: [10.3847/1538-4357/aaa08c](https://doi.org/10.3847/1538-4357/aaa08c)
- Rackham, B. V., Apai, D., & Giampapa, M. S. 2019, *AJ*, 157, 96, doi: [10.3847/1538-3881/aaf892](https://doi.org/10.3847/1538-3881/aaf892)
- Rackham, B. V., & de Wit, J. 2024, *The Astronomical Journal*, 168, 82, doi: [10.3847/1538-3881/ad5833](https://doi.org/10.3847/1538-3881/ad5833)
- Rackham, B. V., Espinoza, N., Berdyugina, S. V., et al. 2023, *RAS Techniques and Instruments*, 2, 148, doi: [10.1093/rasti/rzad009](https://doi.org/10.1093/rasti/rzad009)
- Rackham, B. V., Iyer, A. R., Apai, D., et al. 2026, Submitted to AAS Journals
- Radica, M., Piaulet-Ghorayeb, C., Taylor, J., et al. 2025, *The Astrophysical Journal*, 979, L5, doi: [10.3847/2041-8213/ada381](https://doi.org/10.3847/2041-8213/ada381)
- Ratheke, A. D., Buchhave, L. A., Wit, J. d., et al. 2025, *ApJL*, 979, L19, doi: [10.3847/2041-8213/ada5c7](https://doi.org/10.3847/2041-8213/ada5c7)
- Redfield, S., Endl, M., Cochran, W. D., & Koesterke, L. 2008, *The Astrophysical Journal*, 673, L87, doi: [10.1086/527475](https://doi.org/10.1086/527475)
- Richard, C., Gordon, I. E., Rothman, L. S., et al. 2012, *Journal of Quantitative Spectroscopy and Radiative Transfer*, 113, 1276, doi: [10.1016/j.jqsrt.2011.11.004](https://doi.org/10.1016/j.jqsrt.2011.11.004)
- Rothman, L. S., Gordon, I. E., Barber, R. J., et al. 2010, *Journal of Quantitative Spectroscopy and Radiative Transfer*, 111, 2139, doi: [10.1016/j.jqsrt.2010.05.001](https://doi.org/10.1016/j.jqsrt.2010.05.001)
- Rotman, Y., Welbanks, L., Line, M. R., et al. 2025, arXiv, doi: [10.48550/arXiv.2503.21702](https://doi.org/10.48550/arXiv.2503.21702)
- Schlawin, E., Greene, T. P., Line, M., Fortney, J. J., & Rieke, M. 2018, *The Astronomical Journal*, 156, 40, doi: [10.3847/1538-3881/aac774](https://doi.org/10.3847/1538-3881/aac774)
- Schlawin, E., Ohno, K., Bell, T. J., et al. 2024, *The Astrophysical Journal Letters*, 974, L33, doi: [10.3847/2041-8213/ad7fef](https://doi.org/10.3847/2041-8213/ad7fef)
- Seager, S., & Sasselov, D. D. 2000, *The Astrophysical Journal*, 537, 916, doi: [10.1086/309088](https://doi.org/10.1086/309088)
- Sing, D. K., Désert, J. M., Lecavelier Des Etangs, A., et al. 2009, *Astronomy and Astrophysics*, 505, 891, doi: [10.1051/0004-6361/200912776](https://doi.org/10.1051/0004-6361/200912776)
- Sing, D. K., Pont, F., Aigrain, S., et al. 2011, *Monthly Notices of the Royal Astronomical Society*, 416, 1443, doi: [10.1111/j.1365-2966.2011.19142.x](https://doi.org/10.1111/j.1365-2966.2011.19142.x)
- Sing, D. K., Fortney, J. J., Nikolov, N., et al. 2016, *Nature*, 529, 59, doi: [10.1038/nature16068](https://doi.org/10.1038/nature16068)
- Southworth, J. 2010, *Monthly Notices of the Royal Astronomical Society*, 408, 1689, doi: [10.1111/j.1365-2966.2010.17231.x](https://doi.org/10.1111/j.1365-2966.2010.17231.x)
- Taylor, J., Radica, M., Welbanks, L., et al. 2023, *Monthly Notices of the Royal Astronomical Society*, 524, 817, doi: [10.1093/mnras/stad1547](https://doi.org/10.1093/mnras/stad1547)
- The Astropy Collaboration, Price-Whelan, A. M., Lim, P. L., et al. 2022, *The Astrophysical Journal*, 935, 167, doi: [10.3847/1538-4357/ac7c74](https://doi.org/10.3847/1538-4357/ac7c74)
- Triaud, A. H. M. J., Anderson, D. R., Collier Cameron, A., et al. 2013, *Astronomy & Astrophysics*, Volume 551, id.A80, <NUMPAGES>5</NUMPAGES> pp., 551, A80, doi: [10.1051/0004-6361/201220900](https://doi.org/10.1051/0004-6361/201220900)
- Triaud, A. H. M. J., Gillon, M., Ehrenreich, D., et al. 2015, *Monthly Notices of the Royal Astronomical Society*, 450, 2279, doi: [10.1093/mnras/stv706](https://doi.org/10.1093/mnras/stv706)
- Trotta, R. 2008, *Contemporary Physics*, 49, 71, doi: [10.1080/00107510802066753](https://doi.org/10.1080/00107510802066753)
- Tsai, S.-M., Lee, E. K. H., Powell, D., et al. 2023, *Nature*, 617, 483, doi: [10.1038/s41586-023-05902-2](https://doi.org/10.1038/s41586-023-05902-2)
- Tsiaras, A., Waldmann, I. P., Tinetti, G., Tennyson, J., & Yurchenko, S. N. 2019, *Nature Astronomy*, 3, 1086, doi: [10.1038/s41550-019-0878-9](https://doi.org/10.1038/s41550-019-0878-9)
- Tsiaras, A., Waldmann, I. P., Zingales, T., et al. 2018, *The Astronomical Journal*, 155, 156, doi: [10.3847/1538-3881/aaaf75](https://doi.org/10.3847/1538-3881/aaaf75)
- Underwood, D. S., Tennyson, J., Yurchenko, S. N., et al. 2016, *Monthly Notices of the Royal Astronomical Society*, 459, 3890, doi: [10.1093/mnras/stw849](https://doi.org/10.1093/mnras/stw849)
- Vidal-Madjar, A., Lecavelier des Etangs, A., Désert, J. M., et al. 2003, *Nature*, 422, 143, doi: [10.1038/nature01448](https://doi.org/10.1038/nature01448)
- Vidal-Madjar, A., Désert, J.-M., Lecavelier des Etangs, A., et al. 2004, *The Astrophysical Journal*, 604, L69, doi: [10.1086/383347](https://doi.org/10.1086/383347)
- Wakeford, H. R., & Sing, D. K. 2015, *Astronomy and Astrophysics*, 573, A122, doi: [10.1051/0004-6361/201424207](https://doi.org/10.1051/0004-6361/201424207)
- Wakeford, H. R., Sing, D. K., Kataria, T., et al. 2017, *Science*, 356, 628, doi: [10.1126/science.aah4668](https://doi.org/10.1126/science.aah4668)
- Wakeford, H. R., Sing, D. K., Deming, D., et al. 2018, *The Astronomical Journal*, 155, 29, doi: [10.3847/1538-3881/aa9e4e](https://doi.org/10.3847/1538-3881/aa9e4e)
- Wakeford, H. R., Lewis, N. K., Fowler, J., et al. 2019, *AJ*, 157, 11, doi: [10.3847/1538-3881/aaf04d](https://doi.org/10.3847/1538-3881/aaf04d)
- Wallack, N. L., Batalha, N. E., Alderson, L., et al. 2024, *The Astronomical Journal*, 168, 77, doi: [10.3847/1538-3881/ad3917](https://doi.org/10.3847/1538-3881/ad3917)
- Welbanks, L., & Madhusudhan, N. 2019, *The Astronomical Journal*, 157, 206, doi: [10.3847/1538-3881/ab14de](https://doi.org/10.3847/1538-3881/ab14de)

- Welbanks, L., & Madhusudhan, N. 2021, *The Astrophysical Journal*, 913, 114, doi: [10.3847/1538-4357/abee94](https://doi.org/10.3847/1538-4357/abee94)
- Welbanks, L., Madhusudhan, N., Allard, N. F., et al. 2019, *The Astrophysical Journal*, 887, L20, doi: [10.3847/2041-8213/ab5a89](https://doi.org/10.3847/2041-8213/ab5a89)
- Welbanks, L., McGill, P., Line, M., & Madhusudhan, N. 2023, *The Astronomical Journal*, 165, 112, doi: [10.3847/1538-3881/acab67](https://doi.org/10.3847/1538-3881/acab67)
- Welbanks, L., Bell, T. J., Beatty, T. G., et al. 2024, *Nature*, 630, 836, doi: [10.1038/s41586-024-07514-w](https://doi.org/10.1038/s41586-024-07514-w)
- Welbanks, L., Nixon, M. C., McGill, P., et al. 2025, arXiv, doi: [10.48550/arXiv.2504.21788](https://doi.org/10.48550/arXiv.2504.21788)
- Wiser, L. S., Bell, T. J., Line, M. R., et al. 2025, arXiv, doi: [10.48550/arXiv.2506.01800](https://doi.org/10.48550/arXiv.2506.01800)
- Wong, I., Chachan, Y., Knutson, H. A., et al. 2022, *The Astronomical Journal*, 164, 30, doi: [10.3847/1538-3881/ac7234](https://doi.org/10.3847/1538-3881/ac7234)
- Xue, Q., Bean, J. L., Zhang, M., et al. 2024, *The Astrophysical Journal Letters*, 963, L5, doi: [10.3847/2041-8213/ad2682](https://doi.org/10.3847/2041-8213/ad2682)
- Yurchenko, S. N., Barber, R. J., & Tennyson, J. 2011, *Monthly Notices of the Royal Astronomical Society*, 413, 1828, doi: [10.1111/j.1365-2966.2011.18261.x](https://doi.org/10.1111/j.1365-2966.2011.18261.x)
- Yurchenko, S. N., & Tennyson, J. 2014, *Monthly Notices of the Royal Astronomical Society*, 440, 1649, doi: [10.1093/mnras/stu326](https://doi.org/10.1093/mnras/stu326)
- Zhang, Z., Zhou, Y., Rackham, B. V., & Apai, D. 2018, *AJ*, 156, 178, doi: [10.3847/1538-3881/aade4f](https://doi.org/10.3847/1538-3881/aade4f)
- Öberg, K. I., Murray-Clay, R., & Bergin, E. A. 2011, *The Astrophysical Journal*, 743, L16, doi: [10.1088/2041-8205/743/1/L16](https://doi.org/10.1088/2041-8205/743/1/L16)

## APPENDIX

## A. MODEL PARAMETERS AND PRIORS

Table 2 lists the atmospheric model parameters used to generate synthetic observations and the priors adopted in the retrievals for the Pandora-only observations (see Section 3).

Parameter	HD 209458b <sup>a</sup>	HD 189733b <sup>b</sup>	WASP-80b <sup>c</sup>	HAT-P-18b <sup>d</sup>	K2-18b <sup>e</sup>	Prior
$T_{\text{iso}}$ [K]	1459	1220	825	852	255	$\mathcal{U}[0, 1800]$
$\log(\text{H}_2\text{O})$	-3.0	-3.0	-2.5	-4.3	-3.0	$\mathcal{U}[-12, -1]$
$\log(\text{CH}_4)$	-8.0	-8.0	-3.5	-6.0	-2.0	$\mathcal{U}[-12, -1]$
$\log(\text{CO})$	-4.0	-3.5	-5.0	-4.3	-3.5	$\mathcal{U}[-12, -1]$
$\log(\text{CO}_2)$	-6.0	-5.5	-6.0	-5.0	-4.0	$\mathcal{U}[-12, -1]$
$\log(\text{NH}_3)$	-7.0	-6.5	-5.5	-7.0	-5.5	$\mathcal{U}[-12, -1]$
$\log(\text{H}_2\text{S})$	-4.5	-4.0	-4.0	-5.5	–	$\mathcal{U}[-12, -1]$
$\log(\text{Na})$	-5.5	-5.5	–	–	–	$\mathcal{U}[-12, -1]$
$\log(\text{K})$	-7.0	-7.0	–	–	–	$\mathcal{U}[-12, -1]$
$\phi_{\text{cloud}}$	0.5	0.5	0.4	0.9	0.6	$\mathcal{U}[0, 1]$
$\log P_{\text{cloud}}$ [bar]	1.7	0.5	-7.0	-1.5	-0.5	$\mathcal{U}[-8, 2]$
$\log(a)$	0.0	3.0	0.0	0.0	8.0	$\mathcal{U}[-4, 10]$
$\gamma$	-4.0	-8.0	-4.0	-4.0	-11.0	$\mathcal{U}[-20, 2]$

**Table 2.** Summary of forward-model parameters (columns 2–6) and retrieval priors (last column) used for the models in Section 3. All  $\log(X_i)$  values are molecular abundances given as  $\log_{10}$  volume mixing ratios. The variables for the cloud model described in Section 2.2 are cloud coverage fraction ( $\phi_{\text{cloud}}$ ), the cloud-top pressure ( $\log P_{\text{cloud}}$  in bar), Rayleigh scattering enhancement factor ( $\log(a)$ ), and scattering slope ( $\gamma$ ). “–” indicates a species not included in the model.  $\mathcal{U}$  denotes a uniform prior. Atmospheric abundances roughly follow those from existing studies of these planets with JWST data as a guideline: **a**) Q. Xue et al. (2024), **b**) G. Fu et al. (2024), **c**) T. J. Bell et al. (2023); L. S. Wisner et al. (2025), **d**) M. Fournier-Tondreau et al. (2024a), **e**) N. Madhusudhan et al. (2023).

Table 3 lists the atmospheric model parameters used to generate synthetic observations and the priors adopted in the retrievals for the combined Pandora and JWST observations (see Section 4). These parameters are determined via equilibrium chemistry expectations at the equilibrium temperature of the planet (e.g., J. I. Moses et al. 2013).

Parameter	HD 209458b	HD 189733b	WASP-80b	HAT-P-18b	K2-18b	Prior
$T_{\text{iso}}$ [K]	1459	1220	825	852	255	$\mathcal{U}[0, 1800]$
$\log(\text{H}_2\text{O})$	-2.3	-2.3	-2.0	-2.0	-2.0	$\mathcal{U}[-12, -1]$
$\log(\text{CH}_4)$	-7.0	-5.5	-2.5	-2.5	-2.5	$\mathcal{U}[-12, -1]$
$\log(\text{CO})$	-2.5	-2.5	-4.0	-4.0	–	$\mathcal{U}[-12, -1]$
$\log(\text{CO}_2)$	-5.0	-5.0	-5.5	-5.5	–	$\mathcal{U}[-12, -1]$

**Table 3.** Summary of forward-model parameters and retrieval priors used for the models in Section 4. All  $\log(X_i)$  values are molecular abundances given as  $\log_{10}$  volume mixing ratios. Atmospheric abundances are determined following equilibrium chemistry expectations (e.g., J. I. Moses et al. 2013).

B. CH<sub>4</sub> AND NH<sub>3</sub> CONSTRAINTS FROM PANDORA

Here, we show the posterior distributions of CH<sub>4</sub> and NH<sub>3</sub> obtained with Pandora observations, for both the comprehensive and simple models. Both molecules can be accurately constrained with upper limits on their abundances, with the exception of a full abundance constraint of CH<sub>4</sub> on K2-18 b. NH<sub>3</sub> is additionally mostly constrained for HAT-P-18 b in the case of the simple model, although a tail extends towards the lower end of the prior. The comprehensive model, however, shows an unconstrained posterior that ends in an upper limit, though the upper limit is accurate.

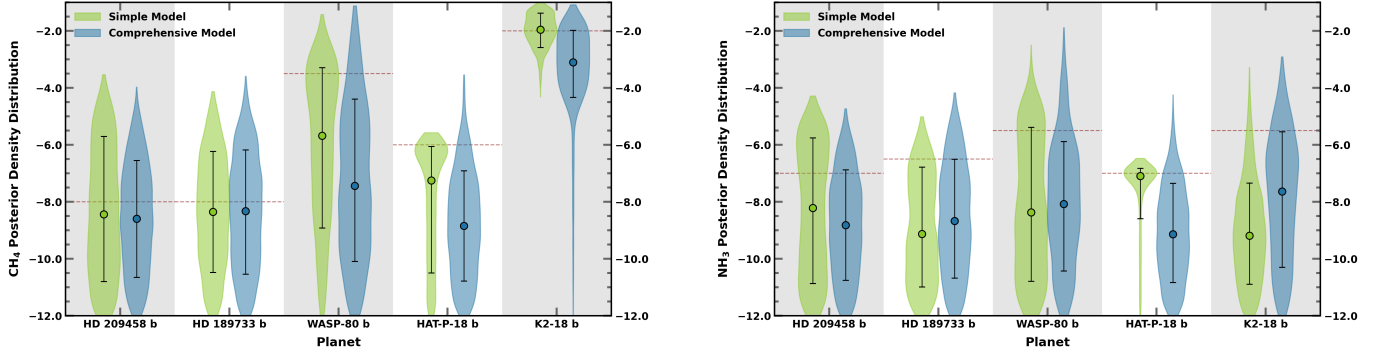


**Figure B1.** Same as Figure 4, but showing the CH<sub>4</sub> (left) and NH<sub>3</sub> (right) abundance constraints from the simple (green) and comprehensive (blue) models.

### C. H<sub>2</sub>O, CH<sub>4</sub>, CO, AND CO<sub>2</sub> CONSTRAINTS FROM PANDORA AND JWST

Here, we show the posterior distributions of H<sub>2</sub>O and CH<sub>4</sub> in Figure C1 and for CO and CO<sub>2</sub> in Figure C2 obtained with Pandora-only, JWST-only, and combined observations, using the comprehensive model for both the data simulation and retrieval. For high CH<sub>4</sub> abundances, Pandora may allow for reliable inferences of the abundance, particularly for high-SNR targets (e.g., HAT-P-18 b and K2-18 b). Notably, despite not containing any strong CO<sub>2</sub> absorption features in the NIRDA bandpass, the inclusion of Pandora data leads to more accurate constraints on CO<sub>2</sub> abundance than JWST alone (particularly for HD 209458 b and HD 189733 b). Additionally, marginal improvement in the CO constraints for the same planets can be seen despite the lack of CO features in the NIRDA bandpass.

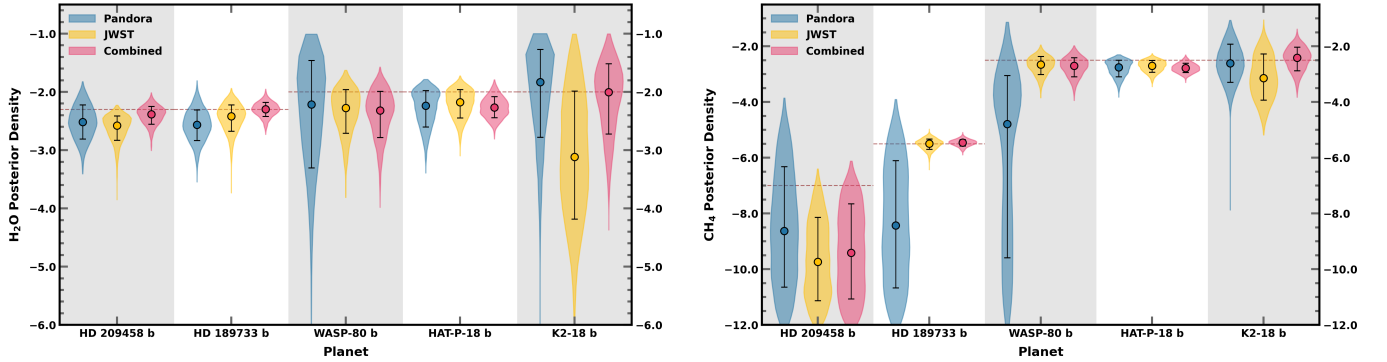


**Figure C1.** Same as Figure 9, but showing the H<sub>2</sub>O (left) and CH<sub>4</sub> (right) constraints from Pandora (blue), JWST (yellow), and combined (pink) data.

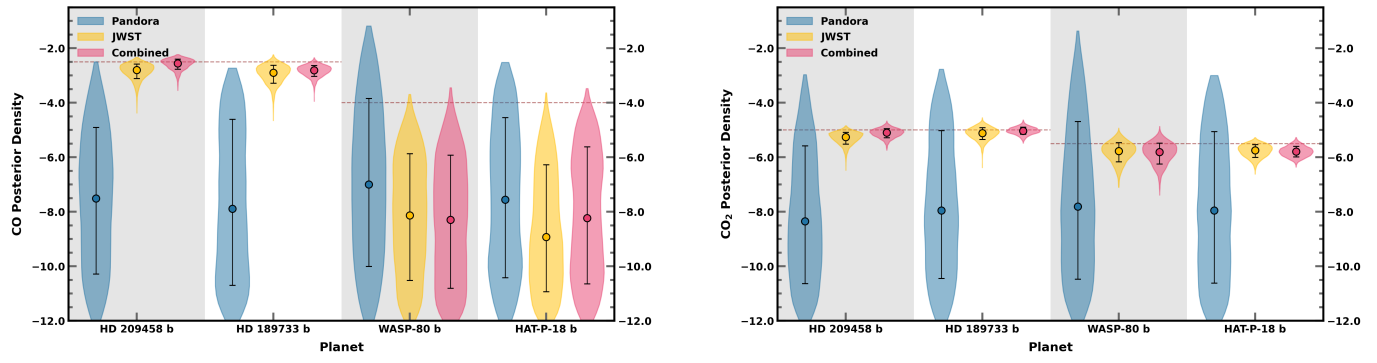


**Figure C2.** Same as Figure 9, but showing the CO (left) and CO<sub>2</sub> (right) abundance constraints from Pandora (blue), JWST (yellow), and combined (pink) data.